AN ANALYTICAL AND EXPERIMENTAL STUDY OF HIGH VELOCITY FLOW IN CURVED SECTIONS OF OPEN CHANNELS

Thesis by

Arthur T. Ippen

Submitted in Partial Fulfillment of the

Requirements for the Degree of Doctor of Philosophy

California Institute of Technology,

Pasadena, California,

1936.

ACKNOWLEDGMENT

This research has been made possible through the initiative of Professor R. T. Knapp and the active cooperation of the Los Angeles County Flood Control District under its Chief Engineer, C. H. Howell, who provided for the financial side of the comprehensive experimental study.

The writer wishes to state here his grateful appreciation of the many helpful suggestions made during the course of his work by Professor R. T. Knapp and Professor Th. von Kármán, to whom a great deal of credit is due if this research should mean a step forward in the science of fluid mechanics.

Mr. W. E. Wilson was connected with the construction of the experimental set-up and the first period of experimentation. Messrs. J. M. Fox and T. W. Griffiths were assisting during the latter period of experimental work and in the evaluation and graphical representation of the great amount of data.

Occasional help and cooperation was given by members of the Engineering Staff of the Los Angeles County Flood Control District.

SUMMARY

In the theory of flow in open channels two stages of flow with principally different characteristics have to be considered, streaming flow and shooting flow. The velocity of flow in the first case is smaller than the velocity of propagation of translatory waves, in the latter case it is larger. The phenomena occurring in streaming flow are well known and theoretically solved, if we neglect the influence of friction. This latter simplification means that the velocity has a constant value for each point of the cross-section. For this assumption also the theory of the hydraulic jump has been successfully attacked, where the stage of flow changes from the shooting to the streaming condition. The present paper, however, deals with problems of flow of the shooting stage only and extends the theory of hydraulics to all cases of supercritical flow, where the variation of depths and velocities due to changes in the direction of flow is desired.

An outstanding example of such a type of flow is the case of curved sections in a rectangular open channel. This case has been investigated in the following analytically by the principles developed, and its solution was then compared to an extensive experimental investigation. It is shown that an adequate solution of the case of high velocity flow in curved sections of open channels has been found.

TABLE OF CONTENTS:

	Page
A. Introduction, Statement of Problem	1
B. Analytical Study of Supercritical Flow	2 - 20
I. Supercritical Flow	2 - 5
a. Definition of Supercritical Flow and Wave Velocity	2
b. Properties of Flow at Supercritical Velocities	4
c. Boundary of Disturbances	5
II. Laws Pertaining to Supercritical Flow	6 - 20
a. Derivation of Wave Angle	6
b. The Influence of a Change in the Direction of Flow	8
1. General Law	8
2. Conditions for Application to Flow in Curves	8
c. Derivation of Elevation Produced by Change in Direction	13 - 17
1. Discussion of Possible Assumptions	13
2. Derivation on the Basis of Constant Energy	14
3. Derivation on the Basis of Constant Velocity	17
d. Derivation of Location and Magnitude of First Maximum	18 - 19
1. Location of Beginning of First Maximum	18
2. Depth in Zone of First Maximum	19
C. Experimental Study	21 - 50
I. Experimental Procedure	21
II. Schedule of Tests	22
III. Graphical Results	27 - 50
a. Water Surface Contour Maps	27
b. Water Surface Profiles Along Channel Walls	31
c. Water Surface Profiles Along Outer Channel Walls	38
d. Cross-Sections of Flow and Velocity Distribution	42

TABLE OF CONTENTS (cont.)

	Page
D. Comparison of Experimental and Analytical Results	51 - 64
I. Comparison of Analytical and Experimental Profile of Rise	51
II. Comparison of Analytical and Experimental Maxima	54
III. The General Pattern of Disturbances Set Up By Curves	59
a. Constancy of Pattern for a Given Channel	60
b. The Spacing of Maxima	61
c. The Number of Maxima in Curve	61
d. Relative Height of Maxima in Downstream Tangent	62
E. General Discussion and Final Conclusions	65 - 68
Appendix	
I. The Experimental Set-Up	69 - 75
The Circulation System	
a . The Discharge Measurement	71
b. The Tilting Platform	73
c. The Experimental Flume	73
d. Portable Testing Instruments	74
II. Field Observations on Flow in Curves	76 - 81
a. Verdugo Wash High Water Marks	76
b. Lower Sycamore Storm Drain	77
c. Rubio Storm Drain	78
d. Summary of Field Checks	81
III. A Short Survey of Literature on High Velocity Flow and on Flow in Curves at Subcritical Velocities	82 - 83

LIST OF FIGURES AND TABLES

Figure		Page
1.	Specific Energy Diagram	2
2.	Paths of Wave Fronts	6
3.	Velocity Vector Diagram for Constant Energy Assumption	15
4.	Velocity Vector Diagram for Constant Velocity Assumption	17
5.	Diagram for Derivation of Location of First Maximum	19
	Water Surface Contour Maps	
6.	Runs 13 and 39, Runs 3 and 32	28
7.	Runs 19c and 28, Run 26	29
8.	Runs 52, 57 and 71	30
	Water Surface Profiles Along Channel Walls	
9.	For 10 foot and 20 foot Radius of Curvature	32
10.	For 40 foot Radius of Curvature	33
11.	For Runs of 1-1/2% Slope	34
12.	Photographs of Run 13	35
13.	Photographs of Runs 11 and 39	36
14.	Photographs of Run 32	37
	Water Surface Profiles Along Outer Channel Walls	
15.	For 10 foot and 20 foot Radius of Curvature	39
16.	For 40 foot Radius of Curvature	40
17.	For Runs of 1-1/2% Slope	41
	Cross-Sections of Flow and Velocity Distributions	
18.	Runs 10 and 13	43
19.	Runs 19c and 26	44
20.	Runs 28 and 32	45
21..	Run 39, Runs 18 and 35-37	46
22.	Runs 52 and 57	47
23.	Run 71	48

LIST OF FIGURES AND TABLES (cont.)

Figure		Page
24.	Photographs of Run 18c	49
25.	Photographs of Runs 35 - 36	50
26.	Photograph of Shape of Rise	51
27.	Diagram of Approximate Solution for Long Radius Curves	59
28.	Wave Crest Diagrams	60
29.	Photographs of Disturbance in Downstream Tangent, Slope 3-1/2%	63
30.	Photographs of Disturbance in Downstream Tangent, Slope 1-1/2%	64
31.	Water Surface Profiles Along Channel Walls, Compound Curves	66
32.	Water Surface Profiles Along Outer Channel Walls, Compound Curves	67
33.	Diagram of Experimental Set-Up	69
34.	Scale Drawing of Experimental Set-Up	70
35.	10" Venturi Meter	71
36.	Venturi Manometer and Regulating Valves	72
37.	Slope Adjustment	73
38.	Entrance Nozzle	74
39.	Point Gauge	74
40.	Pitot Measurement	75
41.	Wall Profiles of Rubio Wash	80

Tables

I.	Complete List of Runs and Corresponding Hydraulic Data	24 - 26
II.	Comparison of Shape of Rise in Depth Along Outer Wall	52 - 53
III.	Comparison of Maximum Depths at Outer Wall	55 - 57

TABLE OF NOTATIONS

(Used in the Discussion of Results and in the Analytical Derivations)

d = variable local depth

d_c = critical depth

d_o = average depth in the channel of approach

h' = maximum depth at the outside wall of the curve

b = width of rectangular section

p = wetted perimeter

m = hydraulic radius

v_o = average velocity in channel of approach

v = variable local velocity

v_c = c = critical velocity = wave velocity or celerity

Q = total discharge

q = discharge per unit width

s = slope of flume along centerline

g = acceleration of gravity = 32.2 ft/sec^2

n = Manning's coefficient of roughness

R = radius of curvature of centerline of flume

θ = central angle of turn

θ_o = central angle from beginning of curve to first maximum

β = variable local value of wave angle

β_o = wave angle at the beginning of the curve

A. INTRODUCTION

The investigation presented in the following started originally as an experimental study, from which information was desired on the behaviour of flow at high velocities in curved sections of open channels. In order to simplify the approach to the problem, the cross-section of the channel was chosen rectangular with zero cross-slope. The range of velocities to be considered was such that at any point the velocity stayed above the critical. For the latter condition, it was found, that the laws and formulae that are used and proven correct for low velocity flow failed to yield any results consistent with the experimental outcome of the study. The theory developed thus far for supercritical velocity deals only with straight flow and parallel streamlines or with the transition from the supercritical to the subcritical stage as encountered in the hydraulic jump. In order to obtain a fundamentally correct basis for the analytical study of the problem of flow in curves at velocities which stay always in the supercritical range, the hydraulic theory had to be extended to cover the case of velocities varying across the width of the channel in direction and magnitude. In other words, the lateral component of the velocity-vector had to be taken into consideration besides the longitudinal one. The vertical component was neglected. Since so far no other attempt exists which deals with the conditions present in this problem, it is well to reconsider generally first the factors governing flows at supercritical velocities and to define clearly the properties.

B. ANALYTICAL STUDY OF SUPERCRITICAL FLOW

I. Supercritical Flow

a. Definition of Supercritical Flow and Wave Velocity. The best illustration for the conditions existing at supercritical velocities is given in Fig. 1, which shows the well-known specific energy diagram plotted for the range of conditions as existed in the experimental investigation. The range covered by the experiments is indicated by the shaded area. The boundaries of this area are: On top and bottom the lines of maximum and minimum discharge, on the left the range of velocities existing at 1½% slope, and on the right that for the 10% slope.

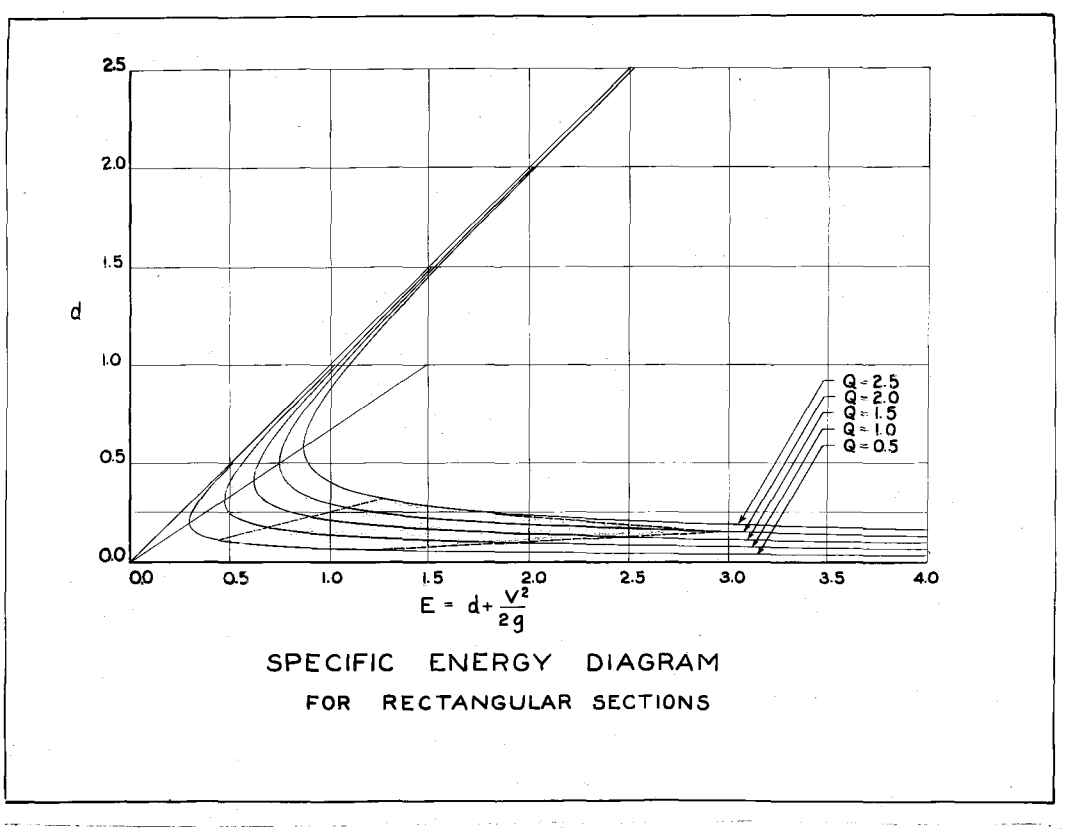

Figure 1

This diagram was obtained by plotting the specific energy defined as $E = d + \frac{v^2}{2g}$ as a function of the depth d. The expression for E can be modified, since $q = vd$, to

$$(1) \qquad E = d + \frac{q^2}{2g d^2}$$

For constant discharges q the curves shown in Fig. 1 can then be drawn. We find that above a certain line, where the slope of the curves changes, all the curves approach asymptotically the straight line $E = d$. The percentage of potential energy as expressed by d in the above relation is here apparently the larger one. If the depth diminishes the value of E depends more and more on the second term in the relation or, in other words, on the velocity head. The point, ~~of inflection~~ where the slope changes of the curves is seen to give the minimum value for the specific energy E. We therefore obtain it by differentiating E with respect to d and by putting the derivative equal to zero. This gives $v = \sqrt{gd}$. The values of d and v obtained by this process are called the critical depth and the critical velocity, respectively. They are defined therefore as the depth and velocity at which a certain discharge can flow with the minimum amount of energy.

The significance of critical velocity for hydraulic problems is augmented by the fact that it is approximately equal to the velocity of propagation of waves. If we assume the wave height infinitely small, the velocity of propagation becomes equal to $c = \sqrt{gd}$. This relation is arrived at by applying the principle of conservation of momentum. Assuming again a constant discharge q per unit width the total momentum M will be

$$M_d = \frac{q}{g} v + \frac{d^2}{2} = \frac{q^2}{gd} + \frac{d^2}{2}$$

If due to some disturbance the depth d is changed to D, the momentum will be $M_D = \frac{q^2}{gD} + \frac{D^2}{2}$. If M_d and M_D are equal, we have a state of equilibrium and the assumed disturbance, where we have the change from d to D, is stationary. We can express this condition also in the following way: the velocity of propagation of the disturbance has become equal to the velocity of flow of the fluid entering into the zone of disturbance. Therefore $\frac{q^2}{gd} + \frac{d^2}{2} = \frac{q^2}{gD} + \frac{D^2}{2}$ and since $q = d \cdot v = V \cdot D$

$$(2) \qquad v = \sqrt{gD}\sqrt{\tfrac{1}{2}\left(1 + \tfrac{D}{d}\right)}$$

We see that only for the relation $\frac{D}{d} = 1$ we obtain theoretically a velocity of propagation $v = c = \sqrt{gD}$ which may also be called celerity. However, practically the numerical value of $\sqrt{\frac{1}{2}\left(1 + \frac{D}{d}\right)}$ differs from unity only for large values of $\frac{D}{d}$. Therefore it is possible that for these cases a wave of large height as compared to the depth can travel upstream even if the velocity of flow is equal to a v somewhat above the critical value $v = \sqrt{gd}$.

The critical velocity of flow and the velocity of propagation of shallow depth water waves coincide only if the wave height can be neglected with regard to the depth.

b. Properties of Flow at Supercritical Velocities. From the definitions given in the previous paragraph we can draw a number

of conclusions which are of decisive value for the problem in question. The most outstanding difference between flows occurring above and below the critical stage is, that disturbances generally cannot be propagated upstream or, in other words, downstream conditions cannot affect upstream ones. The only exception to this rule are waves of large height for the reason discussed in the previous paragraph. Thus, for example, a pier or other obstruction in a stream flowing at supercritical velocity cannot cause an increase in depth at any point at any appreciable distance upstream from the obstruction, unless it does so by causing the flow to pass out of the supercritical range. When this does occur, it is shown by the presence of a hydraulic jump. However, if the flow does remain completely in the field of supercritical velocity, the disturbance is propagated in the direction of flow. This can be represented by a disturbance propagated in all directions from the obstruction with the wave velocity superimposed upon the velocity of flow. Since this latter velocity is always greater than the former, there will be no resultant upstream components. The limits of the disturbance will be a V with the apex at the obstruction, i.e. similar in appearance to the bow wave of a boat. The angle of this V is equal to twice the wave angle.

c. Boundary of Disturbances. The significance of this boundary should be analyzed. Since it is the limit of the disturbance, it follows that no disturbances can be propagated upstream through it, though they are, of course, propagated along it. Therefore it follows that, if the disturbance is caused by a change of velocity

only the change in the component perpendicular to the wave front can produce a change of elevation. These unique properties of supercritical flow hold the key to the solution of many of its problems, of which the flow around curves is one.

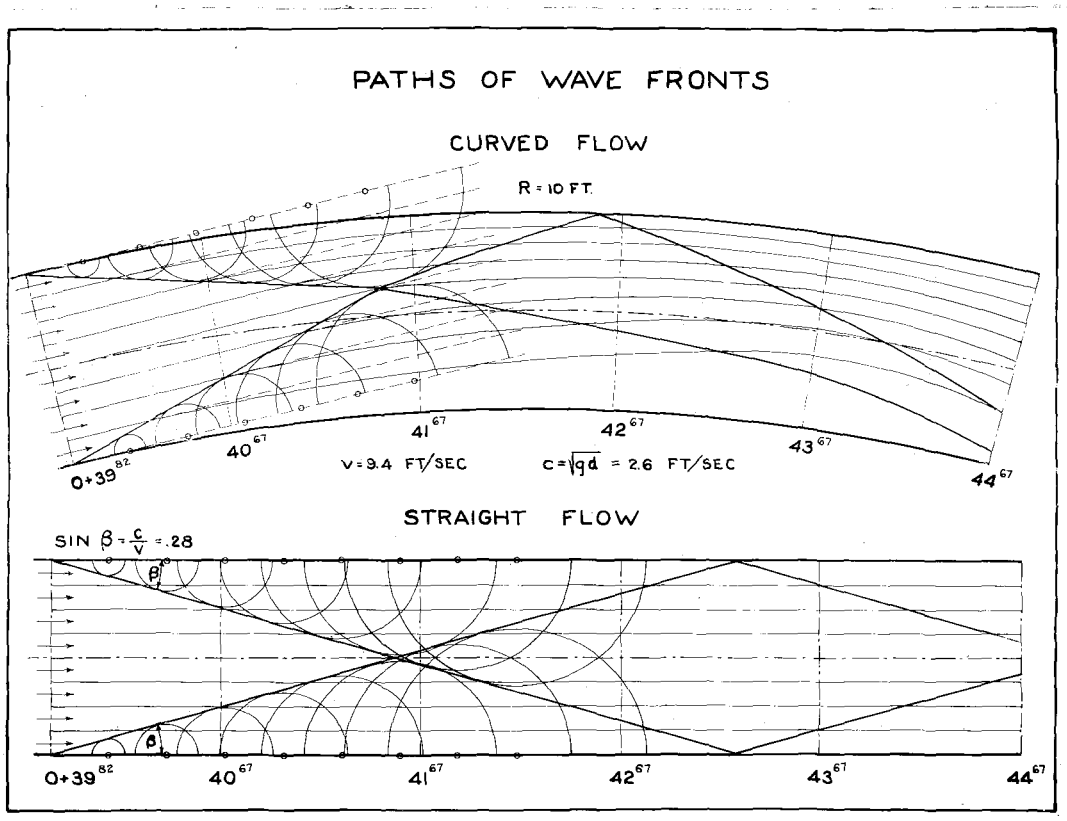

Figure 2

II. Laws Pertaining to Supercritical Flow

a. Derivation of Wave Angle. We are now in a position to analyze the interrelations which must exist in the case of combined flow of water and wave propagation. We know that a stone dropped into still water will cause a circular wave travelling from the point of disturbance with a radial celerity $\sqrt{gd}$. It is easy to

imagine that a rectilinear flow superimposed on this circular wave will distort the circular pattern, since the part of the wave travelling upstream will proceed with a resulting celerity of $\sqrt{gd} - v$ and the part directed downstream with the sum of the two, $\sqrt{gd} + v$. If we accelerate the flow now to a point where $\sqrt{gd} = v = c$, we see that the most the disturbance can do is to send a wave out perpendicular to the direction of flow, while the celerity in the downstream direction has become $c = 2\sqrt{gd}$. If the velocity of flow increases further, the disturbance will be propagated at an angle β to the direction of flow, given by the relation $\sin\beta = \frac{c}{v}$

$\sin\beta = \frac{\sqrt{gd}}{v}$. If the disturbance is a permanent one and the flow conditions are constant, the angle β stays constant too, and we obtain a straight wave front progressing from the source of disturbance at an angle β with the direction of flow, till it is interfered with. If a wave hits a wall, it is reflected and travels back under the same angle β. If two waves cross each other, they do not interfere, unless the water flowing past a wave front has suffered a change in direction or velocity due to a finite wave-height, then the wave crossing into a region of a changed depth and velocity will proceed under a new angle determined from the new values $\sqrt{gd}$ and v.

In the lower part of Fig. 2 is indicated a rectilinear flow in a straight channel of constant velocity and depth. If we cause a small continuous disturbance at the left entrance-section at opposite points of the walls, the wave fronts starting from

these points will form the diamond pattern indicated in the picture. Such patterns have been observed and photographed many times.

If neither the depth nor the velocity and its direction stay constant, but vary as the wave progresses, the pattern of the waves is distorted accordingly and, in the case of a curved flow, assumes the form shown in the upper part of Fig. 2.

b. The Influence of a Change in the Direction of Flow.

1. General Law. The wave lines in Fig. 2 represent only waves of infinitely small size. If we have finite values of wave height, the flow passing under such a wave will undergo a change in velocity and depth in agreement with the law of conservation of momentum. In this case the change of momentum of the water passing the wave is therefore proportional to the change in depth. Further, according to the derivation of the wave velocity, the direction of flow is perpendicular to the wave front, which means that also the acceleration under a wave must be perpendicular to the wave front. If the direction of the flow is oblique to the direction of the wave front, only the component v_n of the velocity normal to the wave front can enter into the problem, while the tangential component v_t remains unchanged. Expressing these statements now in mathematical terms, we have as a further fundamental equation of our problem

$$(3) \qquad \frac{\gamma}{g} v_n \cdot \Delta v_n = -\gamma \Delta d$$

2. Conditions for Application to Flow in Curves. The previous discussion of the fundamental facts of supercritical flow and of the mechanics of pressure translation will be extended to the case of flow through curves. In the literature of Hydraulics so far, no attempt has been made to analyze the case of high velocity

or supercritical, flow in curves. Only the case of lower than critical velocities in curved channels and river bends has been attacked and solved for certain assumptions satisfying within certain limits average natural conditions. The basic assumptions for the formula normally applied to curved flow are the following:

(a) the velocity of flow is constant throughout the cross-section

(b) the direction of the streamlines is parallel to the walls

(c) the velocity of propagation of the disturbance is greater than the velocity of flow.

For these assumptions we can arrive at a solution immediately, since the only forces perpendicular to the flow in a curve are centrifugal force and counteracting it a static pressure force. Calling the difference of the depth at the outside and inside walls h, further assuming an average curvature of the streamlines $1/R$, we can write for a unit length of fluid the following equation of equilibrium: $\frac{mv^2}{R} = \gamma h \cdot d$ wherein h is small against d. Then $\frac{\gamma}{g} b d \frac{v^2}{R} = \gamma \cdot h d$

$$(4) \qquad h = \frac{v^2 b}{R g}$$

We see that according to the derivation not only the previously stated three assumptions have to hold, but also the superelevation h must be small as compared to the total depth d and b must be small against R.

Returning now to the problem of supercritical flow, we find that only the first of the assumptions made for the derivation of

the relation $h = \frac{v^2 b}{R g}$ can be maintained. We may with even better accuracy introduce $v = v_{mean}$, since the velocity distribution tends to become more and more uniform with higher velocities.

The second assumption, however, of all the water moving parallel to the walls cannot be maintained any longer in the light of the previous discussion on the significance of the critical velocity and wave velocity.

In changing the direction of a flowing stream we have to accomplish a change of momentum of the flowing water. This is done by a pressure force proportional to a function of the angle of turn, $f(\Theta)$. This force is built up along the outside bank of a stream, since the velocity vector there has a component directed toward the bank. The same happens along the inside bank with a negative sign however, since the water has the tendency to flow away from the bank. This is identical with the statement that the beginning of a curve must be the beginning of a series of infinitesimal pressure disturbances near the two walls. Remembering that pressure changes can only be transmitted to neighboring sections with a velocity equal to the wave velocity, we can express the distinction between the cases of curved flow above and below the critical velocity and find a new method of attack for curved flow at supercritical velocities.

If the velocity of flow is below and, as in most cases, far below the wave or critical velocity, any pressure change or pressure gradient is communicated upstream and therefore reaches all the streamtubes of the cross-section. All the streamtubes

stay approximately parallel to the bank and continue in curved paths. The formula derived above corresponds therefore to actual conditions and gives, perhaps with some refinements, the true value of h in this case.

In the case of velocities of flow higher than the critical we can state the problem according to the foregoing discussion as follows:

The pressure change along outer and inner wall at the beginning of a curve cannot be communicated over the entire section at once. It reaches neighboring streamtubes only at points downstream, lying along the imaginary wave front, which forms an angle β with the direction of flow as discussed before. Any particle in the stream will therefore keep its direction of flow until it passes under a wave front, where it becomes subject to an acceleration normal to this wave front. The particles moving along the centerline stay longest undisturbed.

The acceleration force affecting a particle passing under a wave front can be negative or positive, the component, v_n, normal to the wave front can be increased or decreased and accordingly the depth below the wave may be higher or lower. This depends only on the boundary conditions. It is evident that a wall curving toward the center of the stream, and therefore obstructing the flow, will cause deceleration of the flow and increase of depth, while a wall curving away from the stream, allowing thereby an expansion of the stream, will cause acceleration and decrease in

depth. Correspondingly we may call these wave lines along which a constant impulse is transmitted from the boundaries, "compression" and "depression waves". A curved channel will give rise to both kinds; compression waves along the outer wall and depression waves along the inner wall. Both compression and depression waves cross the stream and ultimately reach the opposite walls. Since the compression waves give an acceleration toward the wave front and cause an increasing depth, successive waves must converge and the surface slope must become steeper. The depression waves have the opposite properties and therefore successive waves diverge, and the surface slope becomes flatter. In the case of curved channels the two kinds of waves are started on opposite sides and therefore they both turn the streamlines in the same direction. This means that after they intersect the effect of the direction change of the streamlines is added up, while the influence on the depth by one wave is counteracted by that of the other.

The practical application of this to our problem is the following: The depth will rise along the outer wall and decrease along the inner wall until the waves, which started due to the beginning of curvature at the respective opposite walls, have completed crossing the stream. From this point of intersection of wave and wall, the depth change must continue with a reversed sign.

According to this discussion and former statements we are now in a position to determine by mathematical approach the following items:

(a) the shape of rise of the depth along the outer wall of

the curve (also the corresponding drop along inner wall)

(b) the location of the beginning of the maximum depth range

(c) the magnitude of the maximum depth to be expected at the outer wall of a curve.

c. Derivation of Elevation Produced by Change in Direction

1. Discussion of Possible Assumptions. Before we enter into the mathematical derivations, we must gain a somewhat clearer conception of the nature and properties of the assumptions on which these derivations are going to be based. Theoretical fluid mechanics usually deals with frictionless ideal fluid and therefore the next assumption is to neglect the influence of friction. Neglecting frictional influences means to consider a uniform initial velocity over the entire cross-section. This assumption holds in high velocity flow phenomena better than in ordinary cases, since the velocity gradient near the boundaries becomes very steep and the mean velocity approaches more and more the value of the maximum velocity. This can be easily seen from the velocity distributions measured and presented in this report. With frictionless flow assumed, it follows that the energy must be constant, i.e. $E = d + \frac{v^2}{2g}$ is constant for every point in the curve. This assumption implies that, for increasing depths d the velocity v must decrease and vice versa. In the case of flow in curves therefore, the velocity becomes lower at the outer and higher near the inner wall.

However, actual flow conditions with real fluids dictate the

reverse effect: i.e., for the same surface roughness and bed slope the velocity of flow in a given section should increase with increasing depth and vice versa, as may be seen from Chezy's simple equation of flow. ($V = C\sqrt{ms}$)

Velocity measurements made in the course of the experiments all indicate that these two opposing factors approximately cancel each other, with the result that the average velocity remains constant in magnitude around the curve. Therefore, as an alternate to the condition of constant energy, it is logical instead to assume a constant velocity. Thus there are two possible sets of assumptions upon which to base the derivation.

(I) (a) Change in elevation due to change in component of velocity perpendicular to the wave front

(b) Frictionless flow

(c) Energy constant

(II) (a) Change in elevation due to change in component of velocity perpendicular to the wave front

(b) Flow with friction

(c) Magnitude of velocity remains constant although direction changes

(2) Derivation on the Basis of Constant Energy (Set I)

Figure 3 shows the geometrical relations existing between the velocities. Water flowing in the direction AB with a velocity v is forced into a new direction AB' due to the angular change in the direction of the wall.

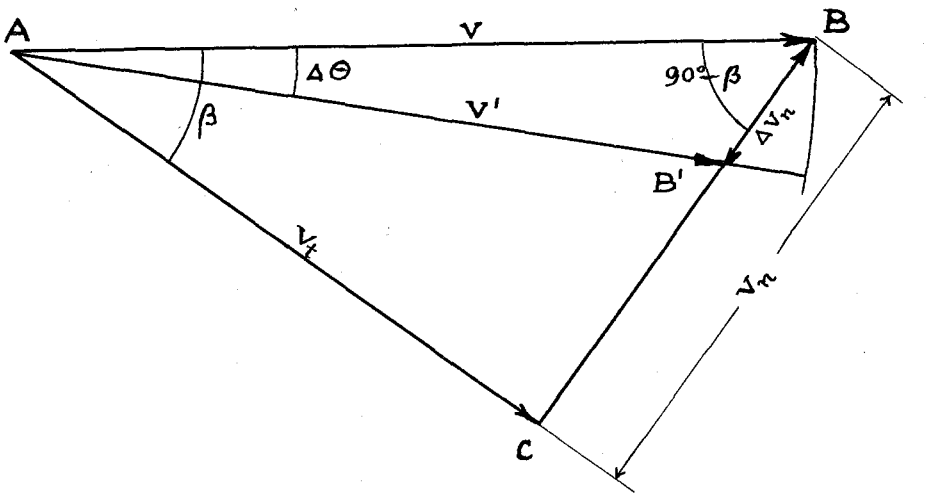

Figure 3

$\overline{AC}$ represents the wave front and v_t and v_n are the components of v, tangential and normal to $\overline{AC}$. According to our former statement (see equation 3)

$$\frac{v_n \, \Delta v_n}{g} = - \Delta d \qquad \text{wherein } v_n = c$$

and from Fig. 3 we obtain

$$(5) \qquad \frac{\Delta v_n}{v} = \frac{\sin \Delta\theta}{\sin (90° - \beta + \Delta\theta)}$$

if we assume the changes $\Delta\theta$ and Δd infinitesimal we have the relations

$$\Delta v_n = - \frac{g \, dd}{v_n}$$

$$\Delta v_n = \frac{v \, d\theta}{\cos \beta}$$

Putting $v_n = v \sin\beta$, we obtain from the two above relations the following differential expression for the depth change.

$$dd = \frac{v^2}{g} \tan\beta \cdot d\theta$$

In this equation β is a function of θ and d and therefore

must be expressed by these terms, in order that the equation may be integrated. From the above Fig. 3 we find

$$\tan\beta = \frac{v_n}{v_t} = \frac{c}{\sqrt{v^2 - c^2}}$$

so that

$$\frac{dd}{d\Theta} = \frac{v^2}{g} \cdot \frac{c}{\sqrt{v^2 - c^2}}$$

Introducing the condition that the total energy must stay constant, i.e.

$$E = d + \frac{v^2}{2g} = \text{const.}$$

or

$$v = \sqrt{2g(E-d)}$$

we can transform the former expression into

$$(6) \qquad \frac{dd}{d\Theta} = \frac{2(E-d)\sqrt{d}}{\sqrt{2E-3d}} \approx \sqrt{2Ed}$$

which is integrable since E = const. If d is neglected against E the approximate form given above is obtained. The integration of the approximate form results in

$$(7) \qquad d = \left(\sqrt{d_o} \pm \sqrt{E/2}\,\Theta\right)^2$$

or

$$\Theta = \sqrt{2}\left(\sqrt{\frac{d}{E}} - \sqrt{\frac{d_o}{E}}\right)$$

The exact integration gives

$$(8) \qquad \Theta + K = \sqrt{3} \cdot \tan^{-1}\sqrt{3}\sqrt{\frac{d/E}{2-3\,d/E}} - \tan^{-1}\sqrt{\frac{d/E}{2-3\,d/E}}$$

$$(8a) \text{ wherein } K = \sqrt{3} \cdot \tan^{-1}\sqrt{3}\sqrt{\frac{d_o/E}{2-3\,d_o/E}} - \tan^{-1}\sqrt{\frac{d_o/E}{2-3\,d_o/E}}$$

The latter relation for Θ and d may be solved best by plotting $\Theta + k$ against d/E. K can be obtained from the same graph for $\Theta = 0$. The limiting cases are:

$$\left(\frac{d}{E}\right)_{max} = \frac{2}{3} \qquad \text{for critical depth}$$

and

$$\left(\frac{d}{E}\right)_{min} = 0$$

3. Derivation on the Basis of Constant Velocity. (Set II)

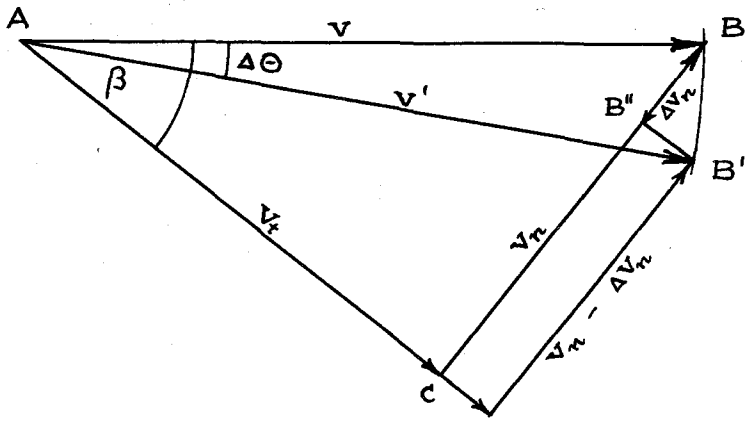

Figure 4

The figure is essentially the same as in case (I). The difference is that in agreement with the stated assumption $V = V'$

$$V_n - \Delta V_n = V \cdot \sin(\beta - \Delta\Theta)$$

$$\Delta V_n = V \cdot \left(\sin\beta - \sin(\beta - \Delta\Theta)\right) \tag{9}$$

From (5) and (9) we obtain for a new equation for Δd :

$$\Delta d = \frac{V^2}{g} \sin\beta \left(\sin\beta - \sin(\beta - \Delta\Theta)\right)$$

$$\Delta d = \frac{V^2}{g} \sin\beta \left[(1 - \cos\Delta\Theta)\sin\beta + \cos\beta \cdot \sin\Delta\Theta\right]$$

assuming again Δd and $\Delta\Theta$ infinitesimal steps we obtain corresponding to equation (6)

$$dd = \frac{V^2}{g} \sin\beta \cdot \cos\beta \cdot d\Theta$$

$$\frac{dd}{d\Theta} = \sqrt{\frac{V^2}{g} - d} \cdot \sqrt{d} \tag{10}$$

The integration gives $\frac{\Theta}{2} + K = \sin^{-1}\sqrt{\frac{gd}{V^2}}$

The boundary conditions are for $\Theta = \sigma$, $d = d_o$ and $\beta = \beta_o$

therefore $$\frac{\Theta}{2} = \sin^{-1}\sqrt{\frac{gd}{V^2}} - \sin^{-1}\sqrt{\frac{gd_o}{V_o^2}}$$

or since $$\sin\beta = \sqrt{\frac{gd}{V^2}}$$

$$(11) \qquad \frac{\Theta}{2} = \beta - \beta_o$$

$$\beta = \frac{\Theta}{2} + \beta_o$$

$$(12) \qquad d = \frac{V^2}{g} \cdot \sin^2\left(\beta_o + \frac{\Theta}{2}\right)$$

d. Derivation of Location and Magnitude of First Maximum.

1. Location of Beginning of First Maximum. Under c were derived formulae which will give the shape and magnitude of the depth change along the outer and inner walls. These formulae hold only as long as there is no influence from the opposite wall. We found before that the point where the first wave from the inner wall reaches the outer is the location of the beginning of the zone of maximum depth. For normal conditions, that is for channels designed so that the depth at the inner wall does not become zero, a close approximation for the location of the point of maximum depth can be obtained by assuming that the wave front starting from the beginning of the curve from the inner wall crosses the stream as a straight line to the point of intersection with the outer wall. The angle between the direction of flow and the wave front is, of course, $= \beta_o$. The total central angle Θ_o from the start A of the wave at the inner wall to the point of intersection B with

the outer wall can then be derived from the geometrical relationship given by Fig. 5.

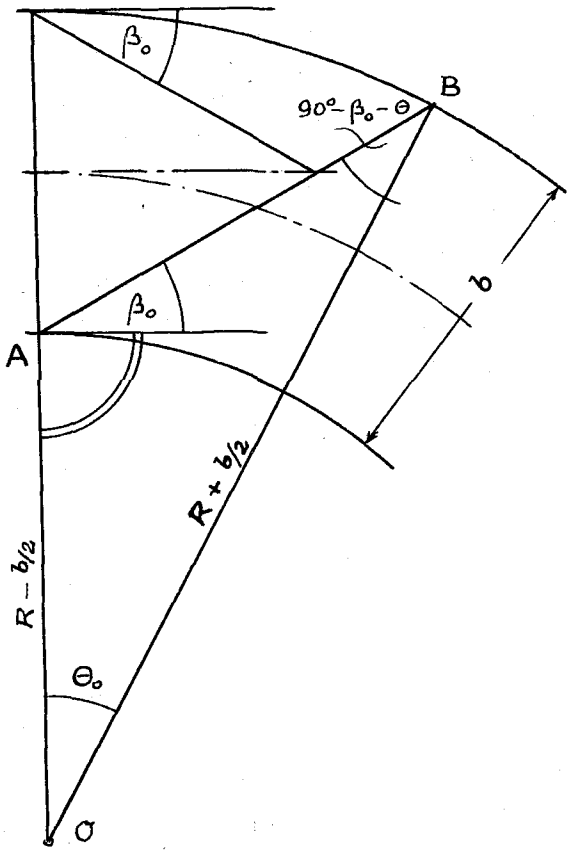

Figure 5

In the triangle AOB we know

$$\sigma A = R - b/2$$

$$\sigma B = R + b/2$$

$$\sphericalangle BA\sigma = 90° + \beta_o$$

We can therefore express the unknown Θ_o by these known quantities with the help of the law of sines.

$$\frac{R - b/2}{R + b/2} = \frac{\sin(90° - \beta_o - \Theta_o)}{\sin(90° + \beta_o)}$$

$$\frac{R - b/2}{R + b/2} = \frac{\cos(\beta_o + \Theta_o)}{\cos\beta_o}$$

from which

$$(13) \qquad \Theta_o = \cos^{-1}\left[\frac{R - b/2}{R + b/2}\cos\beta_o\right] - \beta_o$$

2. Depth in Zone of First Maximum. The maximum depth at the outside wall is now easily determined. Knowing the average depth d_o and the average velocity v_o at the entrance section of the flume the first step is to determine the wave angle β_o

$$\sin\beta_o = \frac{\sqrt{g d_o}}{v_o}$$

T his angle β_o and the proposed curve dimensions R and b are then introduced into relation (13), thus obtaining the central angle θ_o to the point of maximum depth h' .

$$\theta_o = \cos^{-1}\left[\frac{R - b/2}{R + b/2}\cos\beta_o\right] - \beta_o$$

h' may then be calculated with consideration of the initial remarks and statements made under (a) of this chapter from any of the equations derived under (a) by introducing the value of θ_o . It will be found that all of the equations yield sensibly the same result despite the discrepancy in the assumptions on which they are based. This is easily explained when it is remembered that these are all cases of high velocity flow. This is necessarily true for supercritical velocities, because for such velocities $\frac{V^2}{2g}$ is large in comparison to d , therefore even under the assumption of constant energy changes in depth have little power to affect the velocity. Thus the two assumptions are actually nearly equivalent.

C. EXPERIMENTAL STUDY

The experimental program was laid out originally with the idea of making model studies of high velocity flood channels of rectangular cross-section. However, since the range of hydraulic conditions and of dimensions of the proposed prototypes was a very large one, the investigations had to be confined to typical examples of such channels. The general layout of the experimental set-up is clearly seen from the picture opposite the front page. It consists mainly of a platform of 100 ft. length, which can be adjusted to any slope desired from zero to 1 : 10. This platform supports the experimental flume. The technical details with illustrations are given in Appendix I of this paper. In order to make clear the significance of the experimental results as presented mostly in graphical form in the next paragraphs an outline of the procedure and of the extent of the experiments is given here.

I. Experimental Procedure

The typical procedure followed in making an experimental run was:

(1) The platform was adjusted to the approximate slope.

(2) The flume sections were assembled, the curved portion under test being preceded by a straight run of 40 feet in length.

(3) The flume was then adjusted with the help of an engineer's transit, until the centerline was at the proper gradient over the entire length. The maximum deviation from the true grade

was not permitted to exceed 5/1000 of a foot at any point of the 100 foot platform. Simultaneously with this all cross slope was eliminated.

(4) All the joints were made tight and smooth.

(5) A certain flow was established and the movable tongue of the rectangular nozzle was adjusted, until the depth at the entrance of the flume corresponded to the equilibrium depth, as measured just above the curved test section. This was an added insurance that both the velocity and the velocity-distribution were stabilized before the test section was reached.

(6) Water surface profiles were then measured at the various stations, which included four stations above the curved section, 7 to 15 stations in the curved section depending upon its length, and about the same number in the straight section below the curve. This lower straight section was from 20 - 30 ft. long, ie. from 20 - 30 times the channel width.

The above profile readings together with the known quantity of flow and channel slope comprised the necessary data.

(7) The above was repeated for various rates of flow.

(8) In a ddition to the above measurements, velocity distributions were taken during the maximum discharge run.

II. Schedule of Tests

Series of runs similar to that outlined above were made for the combinations listed in tabular form on the following page.

Schedule of Tests

Slope	Radius of Curvature	Central Angle
10%	40'	22.5° and 45°
	20'	45°
	10'	45°
3-1/2%	40'	22.5°
	20'	45°
	10'	45°
1-1/2%	40'	22.5°
	20'	45°
	10'	45°

Table I is a brief summary of the experimental runs performed in accordance with the above schedule together with a subsequent series in which compound curves were used. The latter series begins with Run 78 and extends to the end of the table.

TABLE I.

Run No.	Slope S	Radius R feet	Discharge Q c. f. s.	Average Depth d_o feet	Average Velocity v_o feet	Roughness n
1	.0995	20	1.02	.096	10.62	.0082
2			1.515	.124	12.33	.0082
3			1.988	.150	13.38	.0083
4			1.844	.138	13.37	.0080
5			1.475	.118	12.51	.0078
6			.960	.091	10.55	.0081
7			.480	.055	8.68	.0073
8			1.295	.103	12.54	.0073
9			.705	.070	10.07	.0073
11		10	1.380	.111	12.95	.0076
12			2.048	.147	14.03	.0078
13			2.037	.144	14.16	.0077
14			1.690	.124	13.68	.0074
15			1.015	.091	11.25	.0078
16			.538	.061	8.86	.0077
17			.338	.048	7.12	.0082
18a			.399	.0825	10.23	.0078 *
18a			.391	.180	10.05	.0078 *
18b			.250	.062	8.07	.0081 *
18b			.242	.059	8.28	.0081 *
18c			1.010	.152	13.20	.0083 *
18c			.950	.145	13.20	.0083 *
19c		40	1.985	.146	13.58	.0081
20			1.725	.134	12.85	.0082
21			1.383	.111	12.49	.0076
22			1.000	.089	11.22	.0077
23			.755	.076	9.92	.0077
24			.755	.078	9.62	.0080
25			1.723	.136	12.67	.0083
26			1.983	.146	13.62	.0081
28	.0345		1.973	.200	9.92	.0076
29			1.503	.164	9.18	.0075
30			.950	.123	7.76	.0076
30a		20	1.584	.180	8.86	.0078
32			1.976	.202	9.78	.0078
33			1.015	.128	7.94	.0077
34			.755	.105	7.20	.0077
35		10.25	.517	.138	7.54	.0083 *
35		9.75	.508	.136	7.54	.0083 *
36		10.25	.990	.211	9.45	.0080 *

Note: The width of the flume is b = 1 ft. Runs marked * are for the case of the curved section divided into 2 channels of b = .5 ft.

TABLE I (Cont.)

Run No.	Slope S	Radius R feet	Discharge Q c. f. s.	Average Depth d_o feet	Average Velocity v_o feet	Roughness n
36		9.75	.995	.212	9.45	.0080*
37		10.25	.746	.166	8.98	.0076*
37		9.75	.732	.163	8.98	.0076*
38		10	.767	.109	7.04	.0079
39			1.980	.212	9.36	.0083
41			1.177	.140	8.40	.0074
42			1.500	.169	8.88	.0078
43			1.140	.140	8.17	.0077
44			1.38	.156	8.82	.0076
45			1.685	.184	9.18	.0079
46			1.975	.208	9.48	.0081
47			1.985	.207	9.56	.0080
48	.0155		1.440	.218	6.60	.0081
49		10	.990	.166	5.93	.0079
49		20	.990			
50		10	1.21	.196	6.12	.0082
50		20	1.21			
51		10	1.685	.243	6.94	.0080
51		20	1.685			
52a		10	2.35	.304	7.73	.0080
52a		20	2.35			
52	.0145	10	2.32	.302	7.68	.0080
52		20	2.32			
53		10	.500	.107	4.67	.0079
54		10	2.29	.302	7.58	.0081
55		10	2.145	.284	7.55	.0079
56		10	.74	.137	5.40	.0078
57a		20	2.295	.299	7.68	.0079
57		20	2.305	.298	7.73	.0078
57		10	2.305			
58		20	2.305	.299	7.71	.0078
58		10	2.305			
59		20	1.586	.227	7.00	.0077
59		10	1.586			
60		20	.80	.146	5.49	.0079
60		10	.80			
61		20	1.264	.197	6.42	.0078
61		10	1.264			
62		20	1.995	.273	7.30	.0080
63		20	2.31	.307	7.50	.0082
63		10	2.31			
64		20	.80	.146	5.48	.0079

TABLE I (Cont.)

Run No.	Slope S	Radius R feet	Discharge Q c.f.sec.	Average Depth d_o feet	Average Velocity v_o ft./sec	Roughness n
65	.0145	20	1.630	.240	6.80	.0081
66		40	1.94	.260	7.46	.0076
67			1.355	.196	6.92	.0073
68			0.723	.141	5.13	.0083
69			1.115	.189	5.90	.0084
70			1.68	.240	7.00	.0079
71			2.42	.312	7.76	.0080
72			2.22	.301	7.37	.0082
73			2.01	.285	7.05	.0084
74			1.687	.250	6.75	.0083
75			1.31	.202	6.49	.0079
76			1.00	.172	5.82	.0081
77			0.75	.144	5.21	.0083
78	.0345	40(7.5°)	1.50	.173	8.68	.0082
79		+10(25°)	1.00	.131	7.65	.0080
80			2.40	.239	10.04	.0081
81			1.975	.202	9.78	.0078
82			0.50	.084	5.95	.0081
83		10(25°)	1.00	.132	7.58	.0081
84		+40(7.5°)	2.41	.237	10.16	.0081
85		20(15°)	1.50	.172	8.72	.0080
86		+10(20°)	2.11	.220	9.60	.0082
87			2.4	.243	9.88	.0083
88			1.00	.135	7.42	.0083
89			1.975	.204	9.68	.0079
90		20(15°)	1.97	.210	9.38	.0082
91		+10(25°)	2.40	.240	10.00	.0082
92			1.5	.176	8.53	.0083
93			1.02	.135	7.54	.0082

III. Graphical Results

The graphical results are presented in four series of diagrams as follows:

(a) Water Surface Contour Maps. Figures 6, 7, and 8 all present the water surface contours in and below the test curves for the various radii and gradients employed. It should be noticed that all of the diagrams are for high rates of flow. In order to more clearly present the information, the relative width of the channel has been distorted six to one, i.e. it has been increased to six times normal width. Special notice should be paid to location and the even spacing of the maxima.

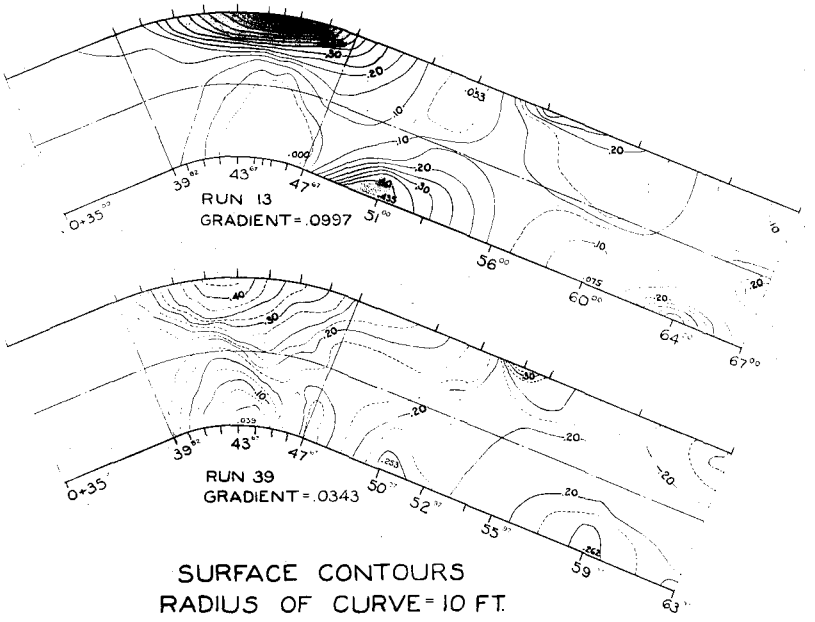

SURFACE CONTOURS
RADIUS OF CURVE = 10 FT.
RUN 13 Q = 2.037 C.F.S.
RUN 39 Q = 1.980 C.F.S.
b = 1. FT.

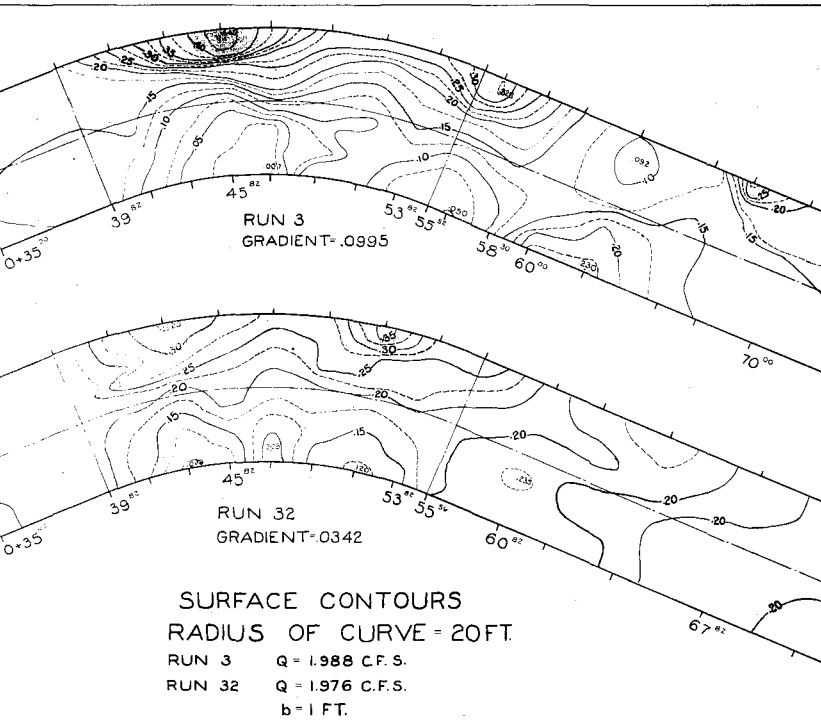

SURFACE CONTOURS
RADIUS OF CURVE = 20FT.
RUN 3 Q = 1.988 C.F.S.
RUN 32 Q = 1.976 C.F.S.
b = 1 FT.

Figure 6

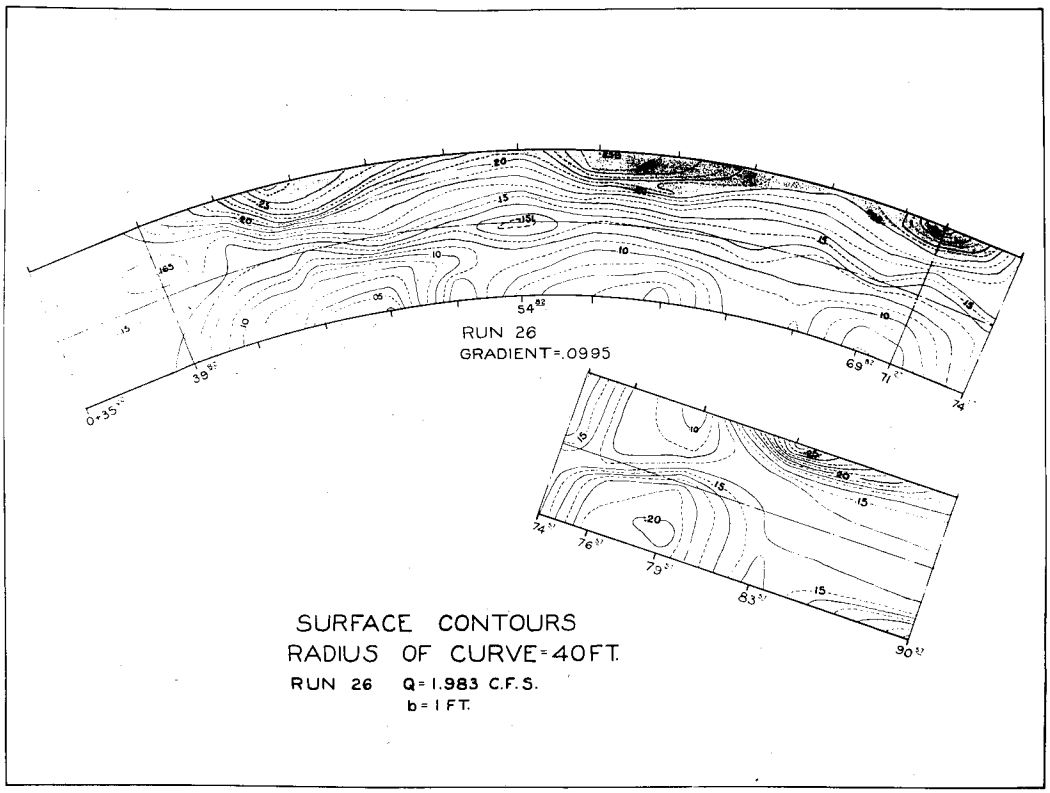

SURFACE CONTOURS
RADIUS OF CURVE=40FT.
RUN 26 Q=1.983 C.F.S.
b=1 FT.

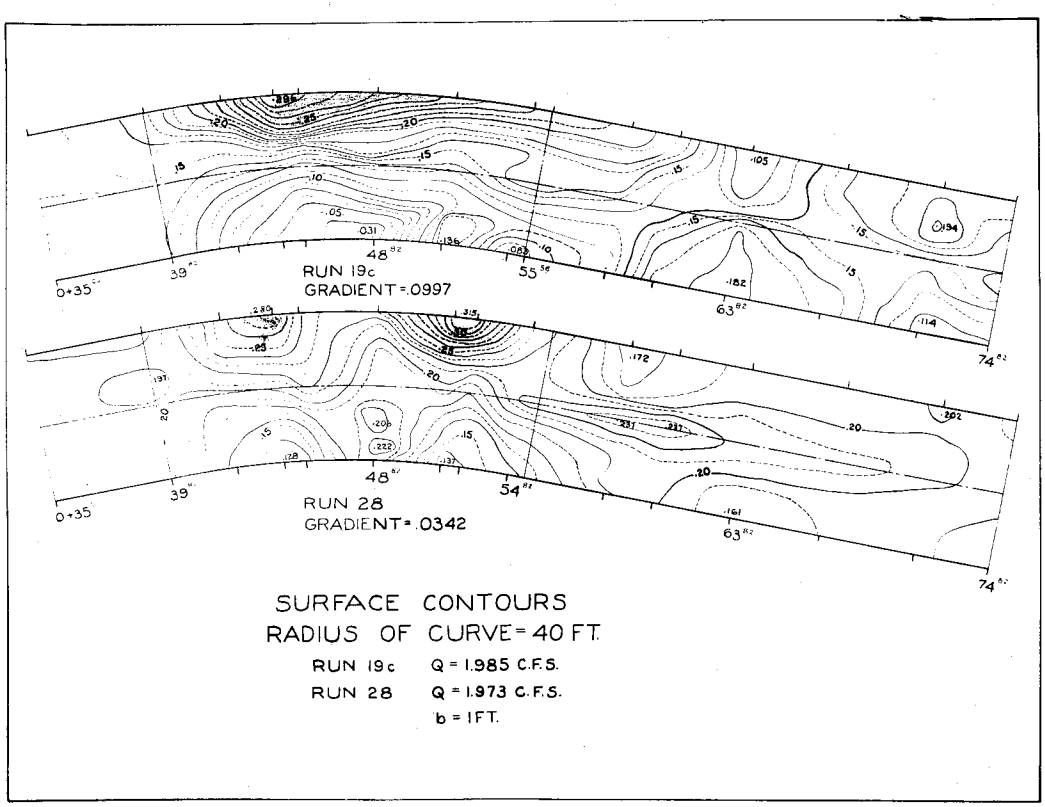

SURFACE CONTOURS
RADIUS OF CURVE=40 FT.
RUN 19c Q=1.985 C.F.S.
RUN 28 Q=1.973 C.F.S.
b=1FT.

Figure 7

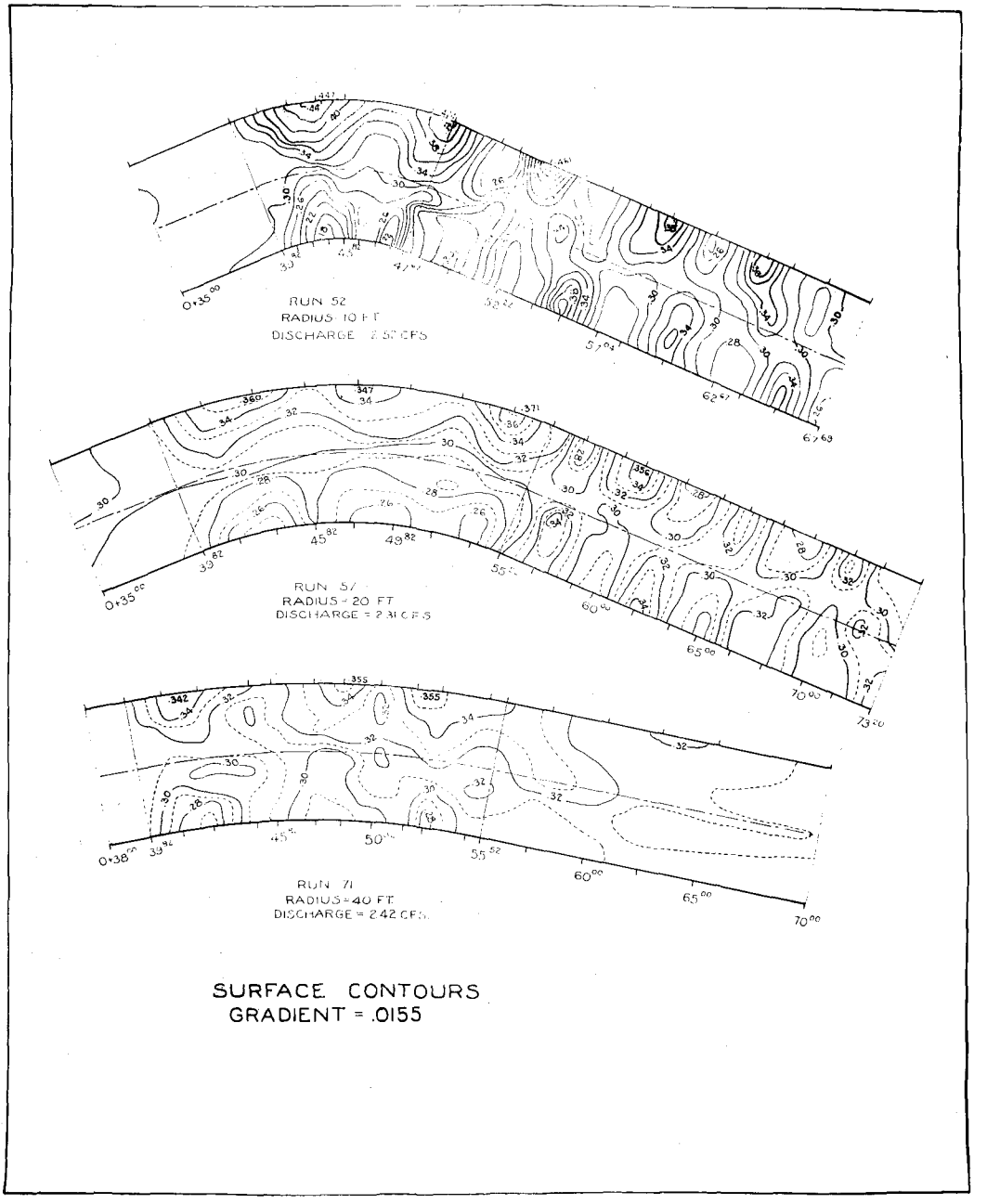
RUN 52
RADIUS 10 FT
DISCHARGE 2.57 CFS
RUN 57
RADIUS = 20 FT
DISCHARGE = 2.31 CFS
RUN 71
RADIUS = 40 FT
DISCHARGE = 2.42 CFS.
SURFACE CONTOURS
GRADIENT = .0155

Figure 8

(b) Water Surface Profiles Along Channel Walls. Figures 9, 10, and 11 show the water surface profiles along the outer and inner walls for the same runs whose contours are seen in Figures 6, 7, and 8. It will be found easier to observe the relative depths from these profiles than from the contours. Attention is called to the relative heights of the maxima in the downstream straight sections in comparison to those in the curves. Figures 12 and 13 are photographs of some of the typical runs. Inspection of the pictures of figure 14 will show the appearance of two maxima in the curved portion of the channel. These are both in the 20 ft. radius curve with a gradient of 3-1/2%.

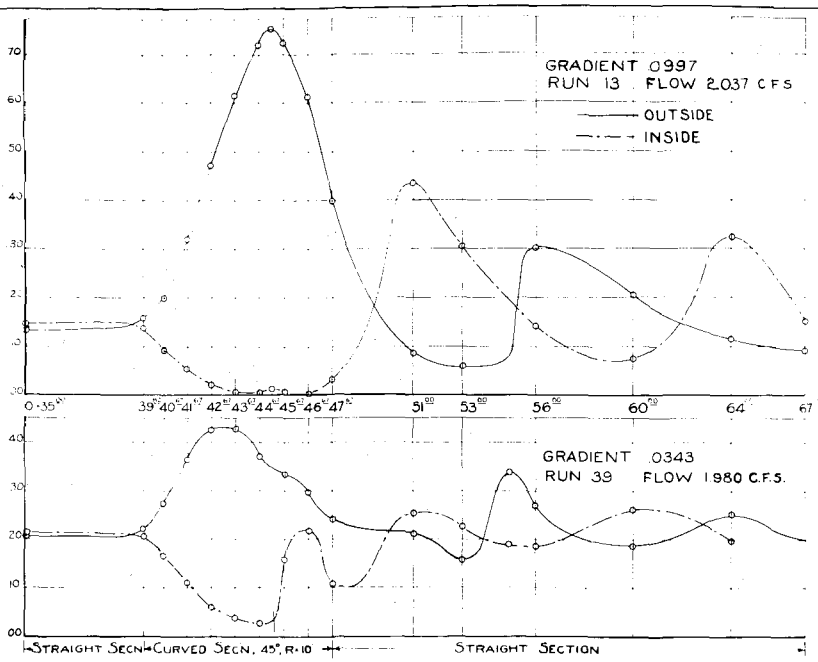

WATER SURFACE PROFILES
ALONG CHANNEL WALLS
RADIUS OF CURVE 10 FT.

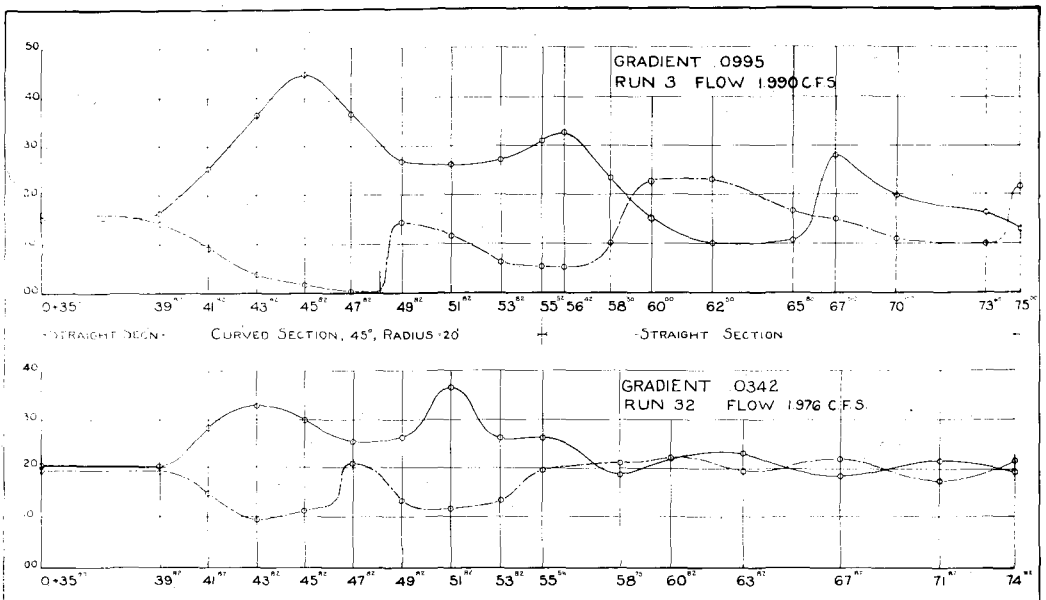

WATER SURFACE PROFILES
ALONG CHANNEL WALLS
RADIUS OF CURVE 20 FT.

OUTSIDE
INSIDE

Figure 9

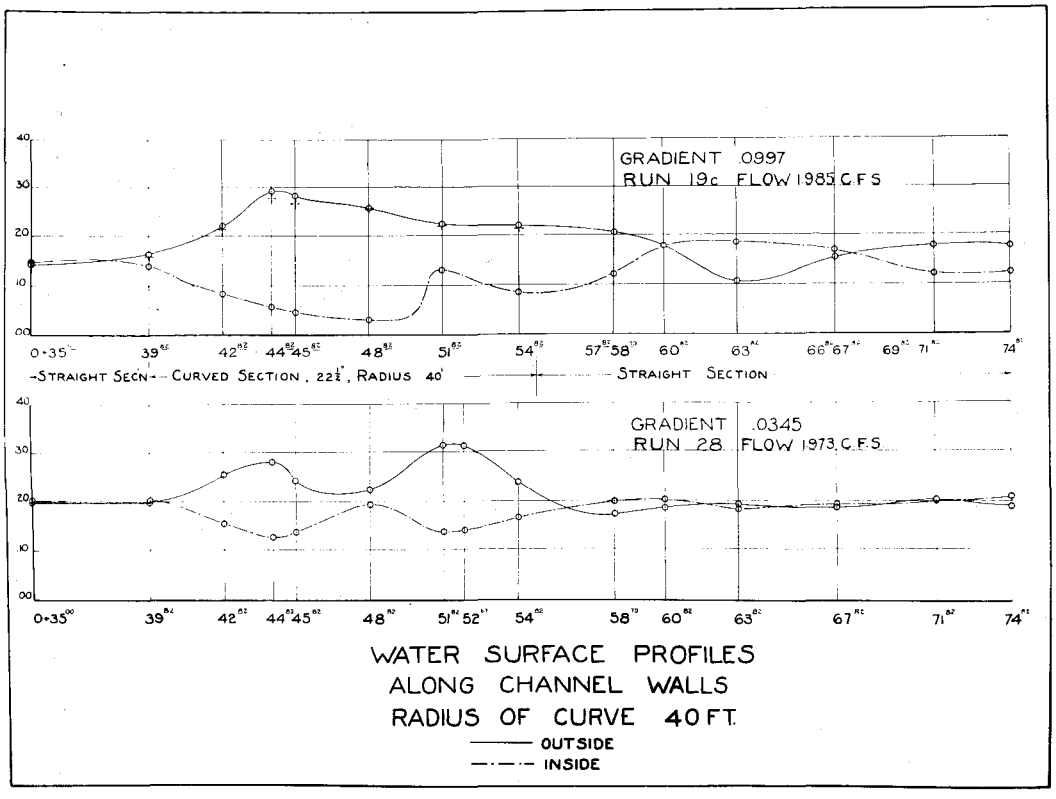

WATER SURFACE PROFILES
ALONG CHANNEL WALLS
RADIUS OF CURVE 40 FT.

——— OUTSIDE
—·—·— INSIDE

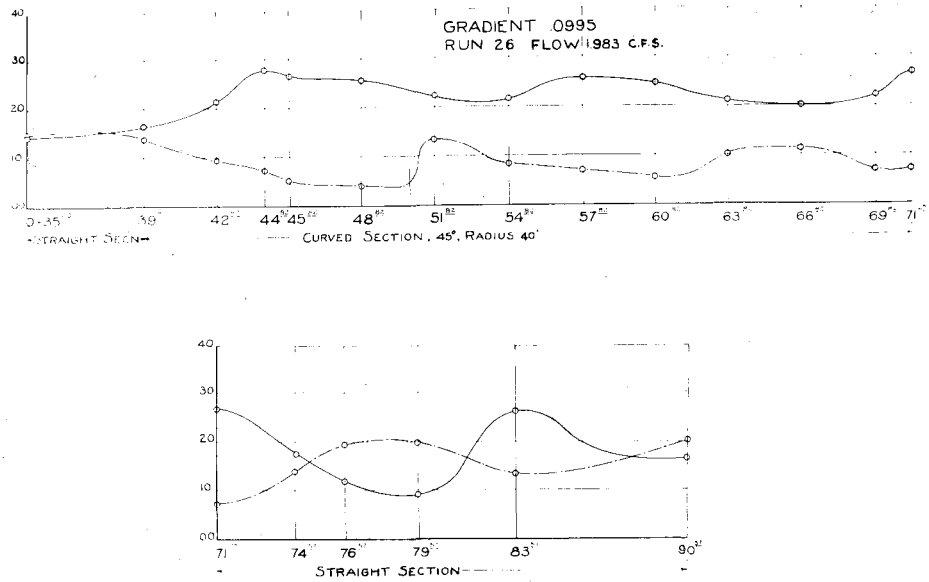

WATER SURFACE PROFILES
ALONG CHANNEL WALLS
RADIUS OF CURVE 40 FT.

——— OUTSIDE —·—·— INSIDE

Figure 10

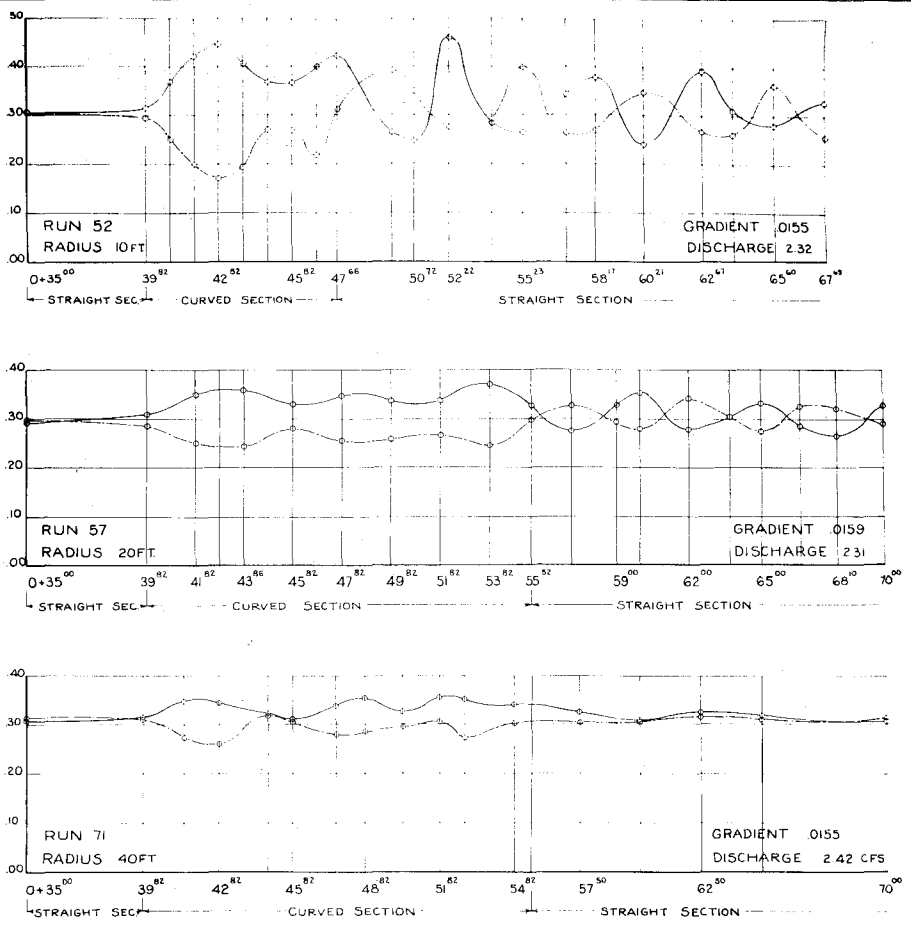
RUN 52
RADIUS 10FT
GRADIENT .0155
DISCHARGE 2.32
STRAIGHT SEC.
CURVED SECTION
STRAIGHT SECTION
RUN 57
RADIUS 20FT
GRADIENT .0159
DISCHARGE 2.31
STRAIGHT SEC.
CURVED SECTION
STRAIGHT SECTION
RUN 71
RADIUS 40FT
GRADIENT .0155
DISCHARGE 2.42 CFS
STRAIGHT SEC.
CURVED SECTION
STRAIGHT SECTION
WATER SURFACE PROFILES
ALONG CHANNEL WALLS
OUTSIDE
INSIDE

Figure 11

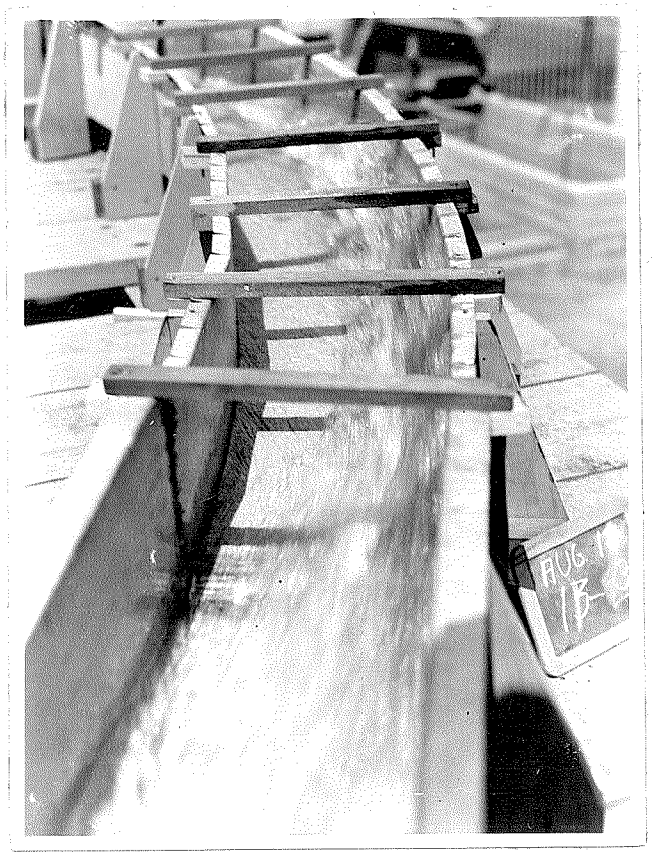

a. Looking upstream into curve.

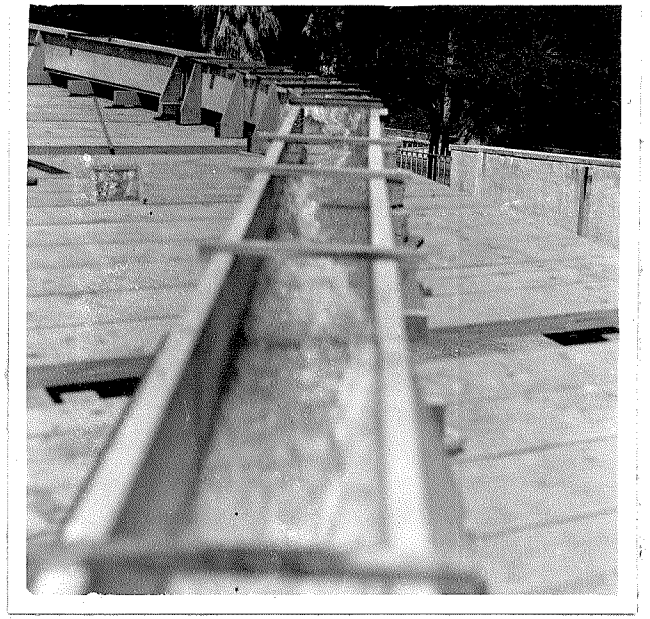

b. Looking upstream into straight section below curve.

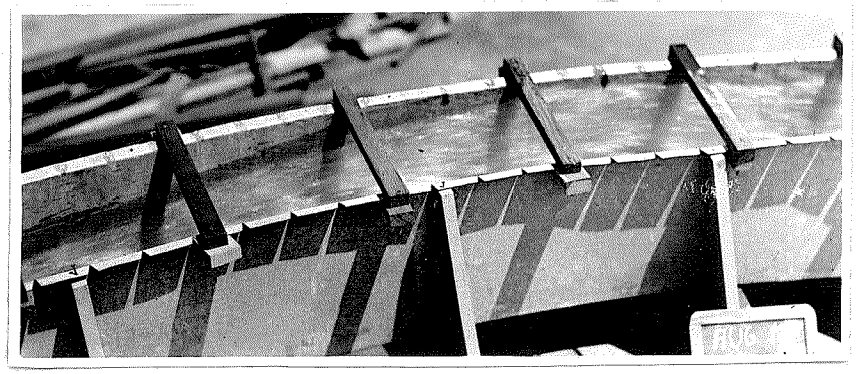

c. Rise of depth along outside wall to maximum.

Figure 12 Run 13, 10 foot radius, 45°
Gradient .0997, Discharge 2.037 c.f.s.

a. Run 11, 10 foot radius, 45°.
Gradient .0995, Discharge 1.38 c.f.s.

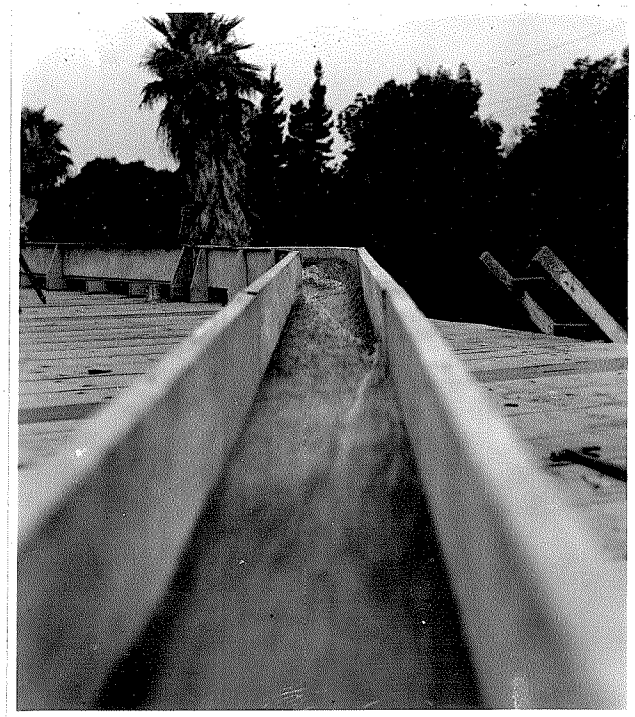

b. Run 11, conditions as before, looking upstream into straight section below curve.

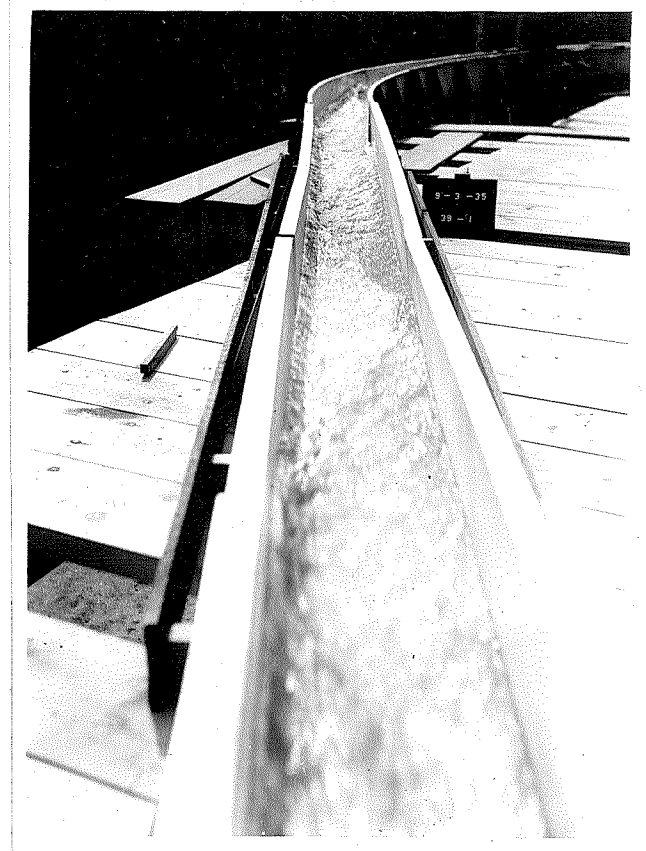

c. Run 39, Discharge 1.985 c.f.s.
Gradient .0343
Disturbance below second curve.
Compare type of waves.

Figure 13

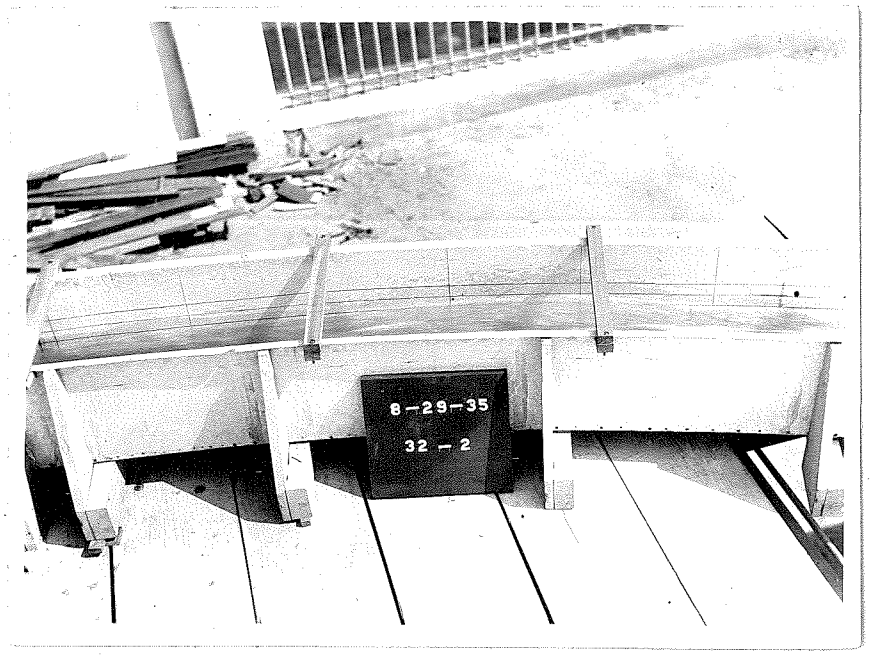

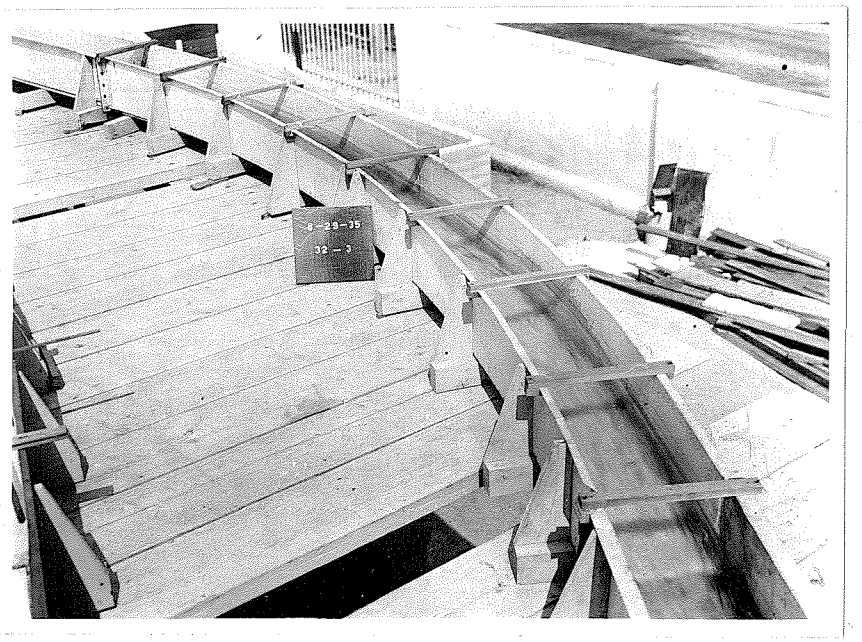

Figure 14 Run 32, 20 foot radius, 45°.
Gradient .0342, Discharge 1.976 c.f.s.
Note the second maximum.

(c) Water Surface Profiles Along Outer Channel Walls

Figures 15, 16 and 17 are also diagrams of the water surface profiles. In these, however, only the profiles along the outer wall are shown. Each diagram consists of all the runs taken with a given test section at one gradient. Each set covers a wide range of discharges. The most striking point brought out by this presentation is that the locations of the maxima in one given channel setting vary very little with change in the rate of flow. However, a gradient change also changes the location of the maxima, which move downstream as the gradient and the velocity are increased. It will also be noticed that, for the same gradient, the points of maxima move downstream slightly as the radius of curvature increases.

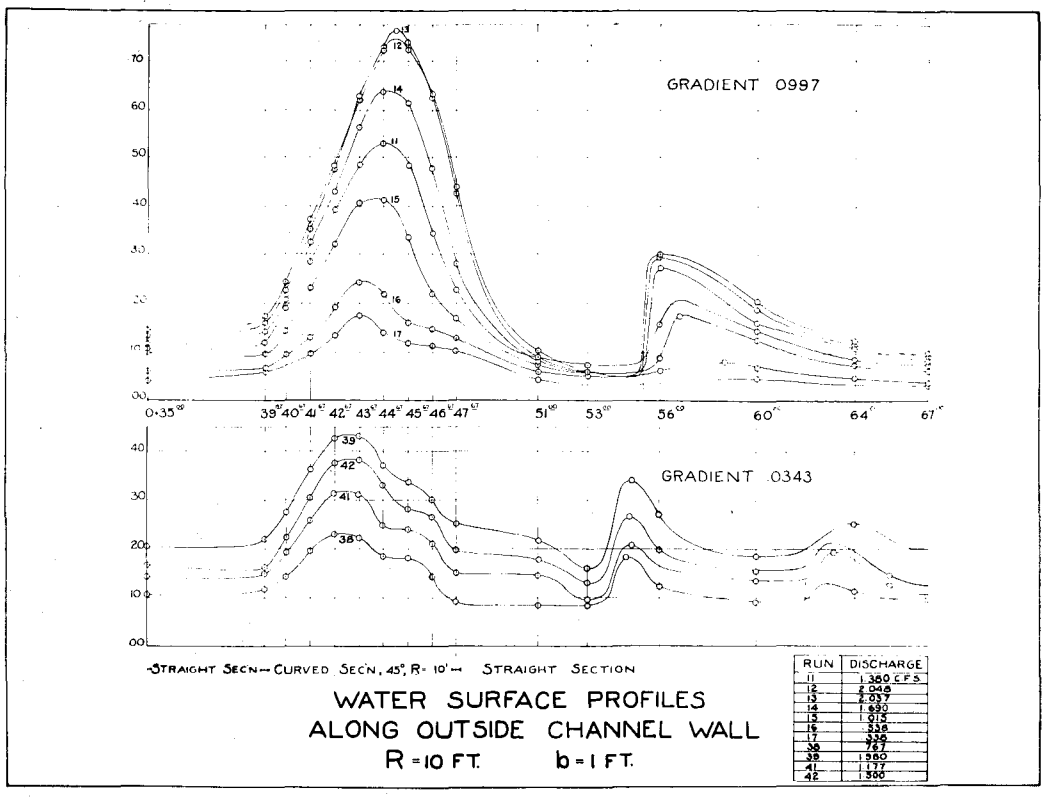
GRADIENT 0997
GRADIENT .0343
STRAIGHT SECN— CURVED SECN, 45°, R= 10' —STRAIGHT SECTION
WATER SURFACE PROFILES
ALONG OUTSIDE CHANNEL WALL
R = 10 FT. b = 1 FT.
RUN | DISCHARGE
11 | 1.360 CFS
12 | 2.046
13 | 2.057
14 | 1.690
15 | 1.015
16 | .338
17 | .325
38 | .767
39 | 1.980
41 | 1.177
42 | 1.300

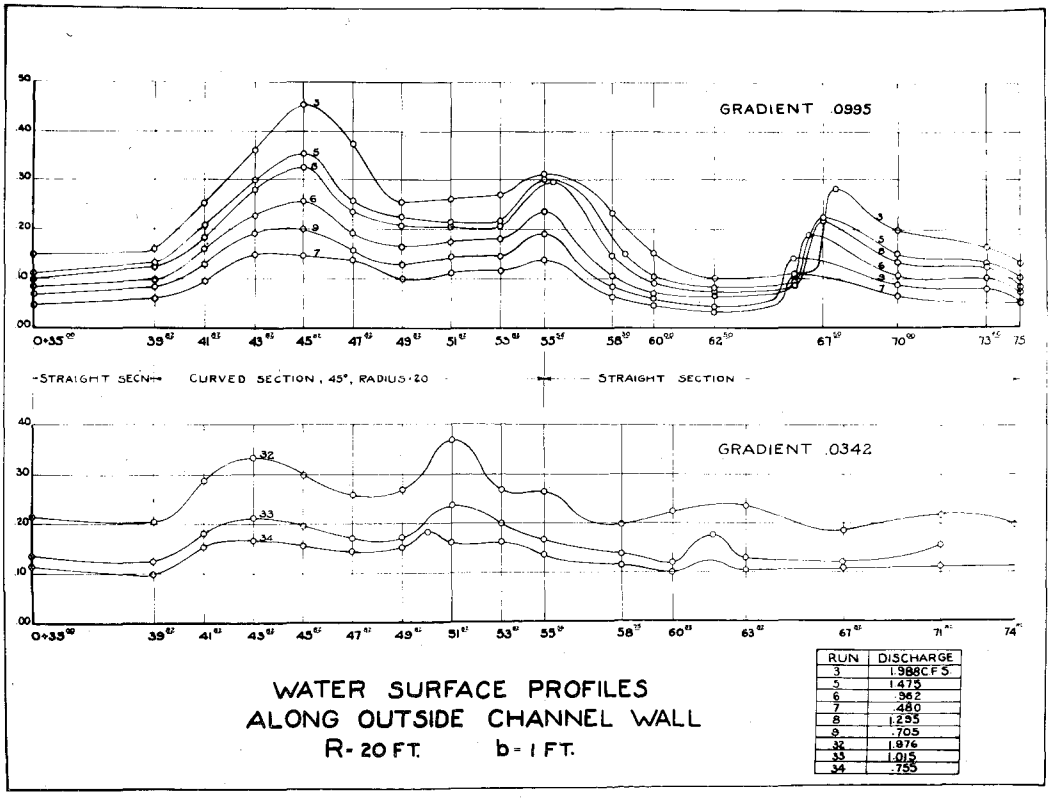
GRADIENT .0995
STRAIGHT SECN— CURVED SECTION, 45°, RADIUS·20 — STRAIGHT SECTION
GRADIENT .0342
WATER SURFACE PROFILES
ALONG OUTSIDE CHANNEL WALL
R- 20 FT. b = 1 FT.
RUN | DISCHARGE
3 | 1.988CFS
5 | 1.475
6 | .962
7 | .480
8 | 1.295
9 | .705
32 | 1.076
33 | 1.015
34 | .755

Figure 15

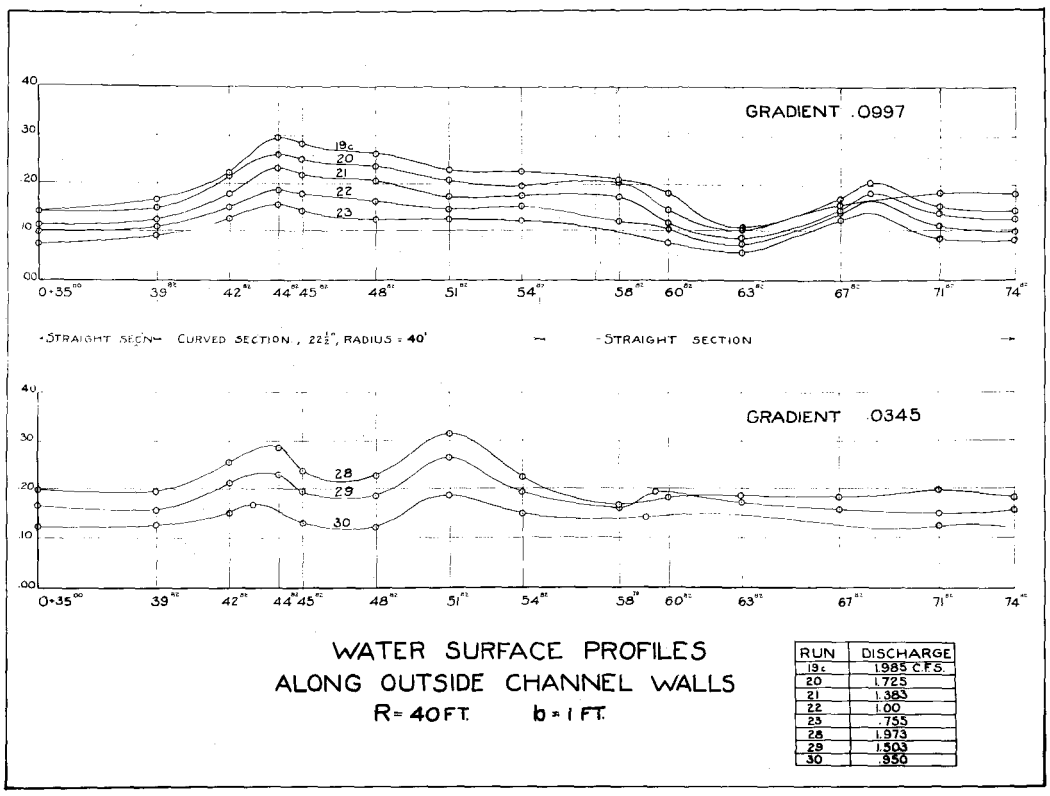

WATER SURFACE PROFILES
ALONG OUTSIDE CHANNEL WALLS
R = 40 FT. b = 1 FT.

RUN	DISCHARGE
19c	1.985 C.F.S.
20	1.725
21	1.383
22	1.00
23	.755
28	1.973
29	1.503
30	.950

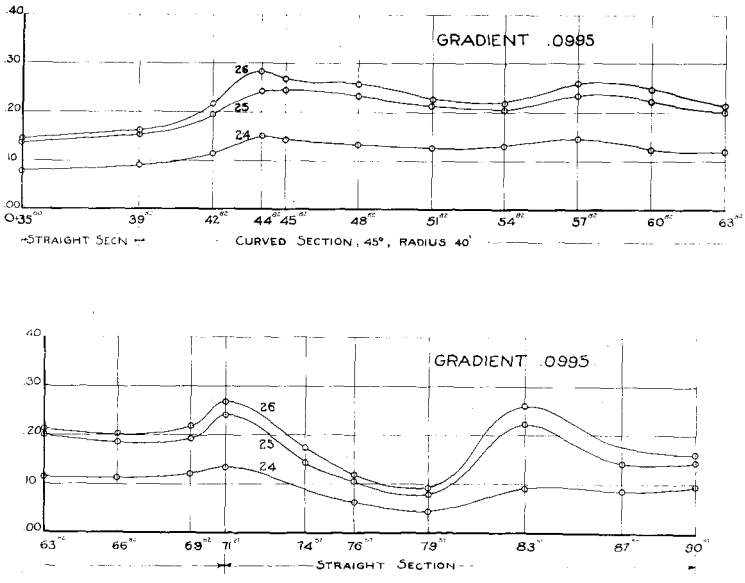

WATER SURFACE PROFILES
ALONG OUTSIDE CHANNEL WALL
R = 40 FT. b = 1 FT.

RUN	DISCHARGE
24	.755 C.F.S.
25	1.723
26	1.983

Figure 16

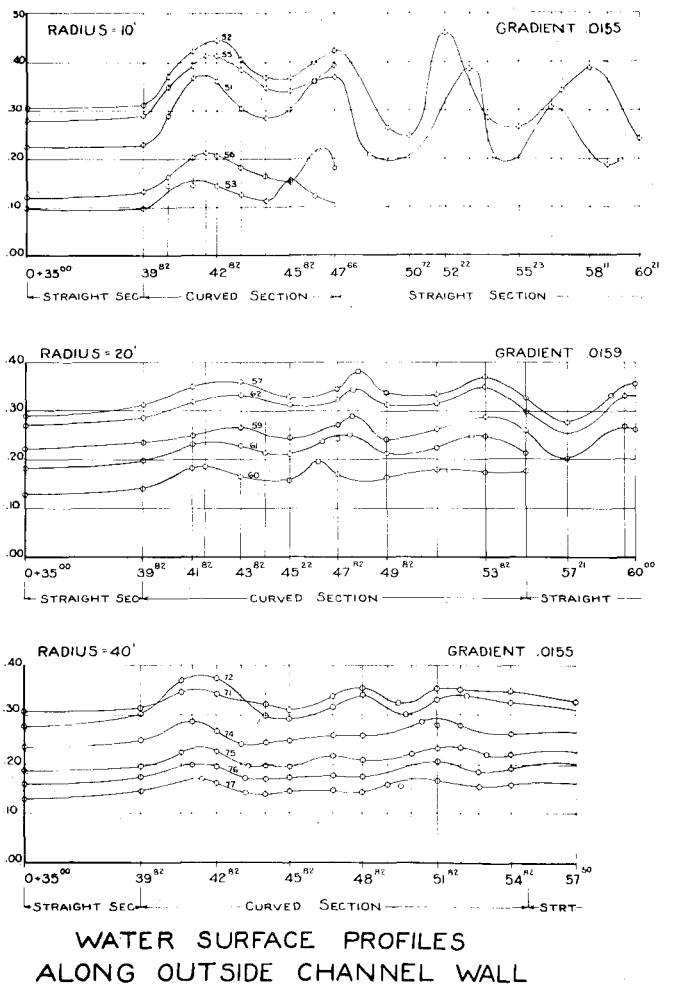

WATER SURFACE PROFILES
ALONG OUTSIDE CHANNEL WALL

Figure 17

(d) Cross-Sections of Flow and Velocity Distributions. Figures 18 to 23 inclusive show cross-sections at the different measuring stations for the maximum discharge runs whose other characteristics have been shown in figures 6 to 11. The vertical scale is distorted two to one. The contour lines show the velocity distributions in the sections measured. Two things should be noticed; first that the velocity distribution at the entrance to the curve is very symmetrical and uniform; and second, that very little change in the average velocity can be observed in the sections taken through points of maximum depth in the curve or in the downstream straight section. This is further shown by the fact that the planimetered cross-section shows a constant area at all stations from the entrance of the curve to the furthermost downstream station measured.

Figure 21 shows a group of profiles taken from a special set of runs. A partition wall was placed in the center of the channel, converting it into two smaller ones. Figures 24 and 25 show photographs of the same set-up. These runs should be considered mainly qualitative, since the set-up was not complete enough to secure uniform conditions at entrance to and in the test section.

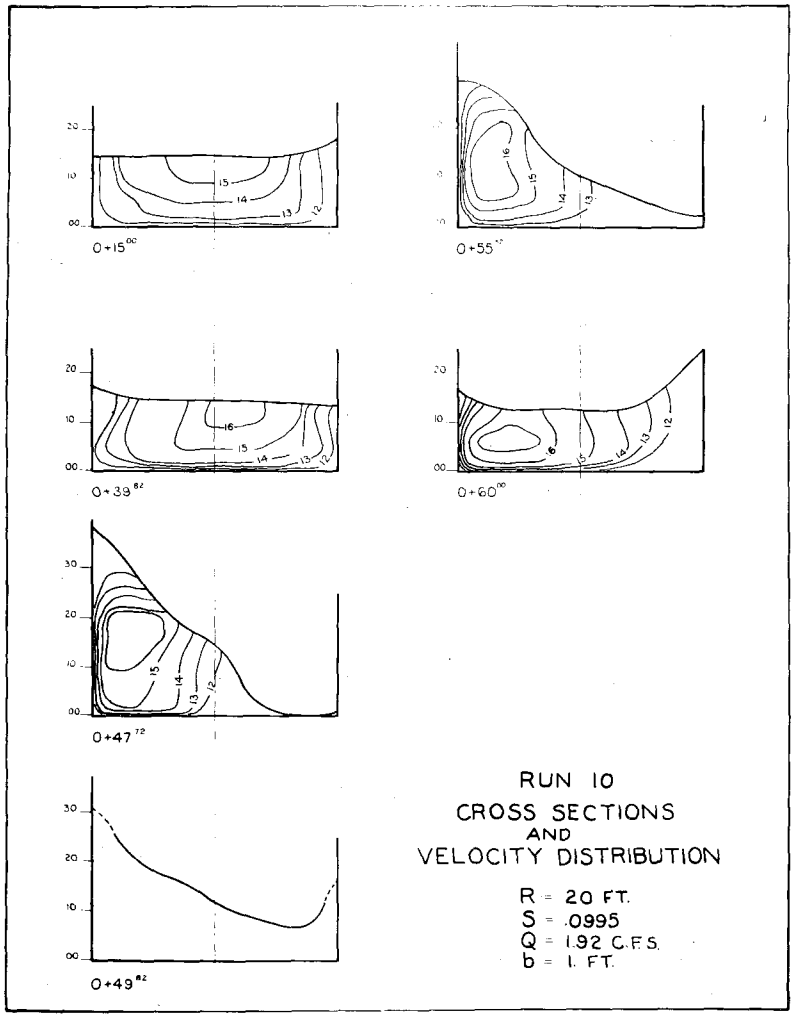
0+15 00
0+55 00
0+39 82
0+60 00
0+47 72
0+49 82
RUN 10
CROSS SECTIONS
AND
VELOCITY DISTRIBUTION
R = 20 FT.
S = .0995
Q = 1.92 C.F.S.
b = 1. FT.

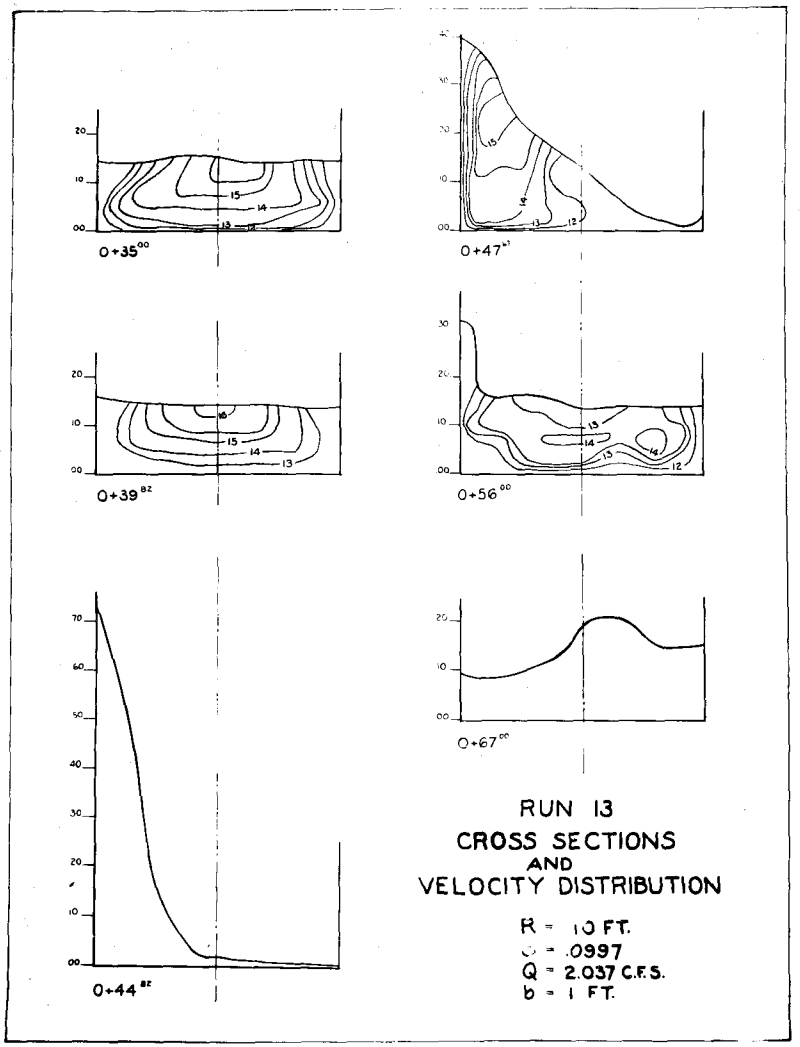
0+35 00
0+47 00
0+39 82
0+56 00
0+44 82
0+67 00
RUN 13
CROSS SECTIONS
AND
VELOCITY DISTRIBUTION
R = 10 FT.
S = .0997
Q = 2.037 C.F.S.
b = 1 FT.

Figure 18

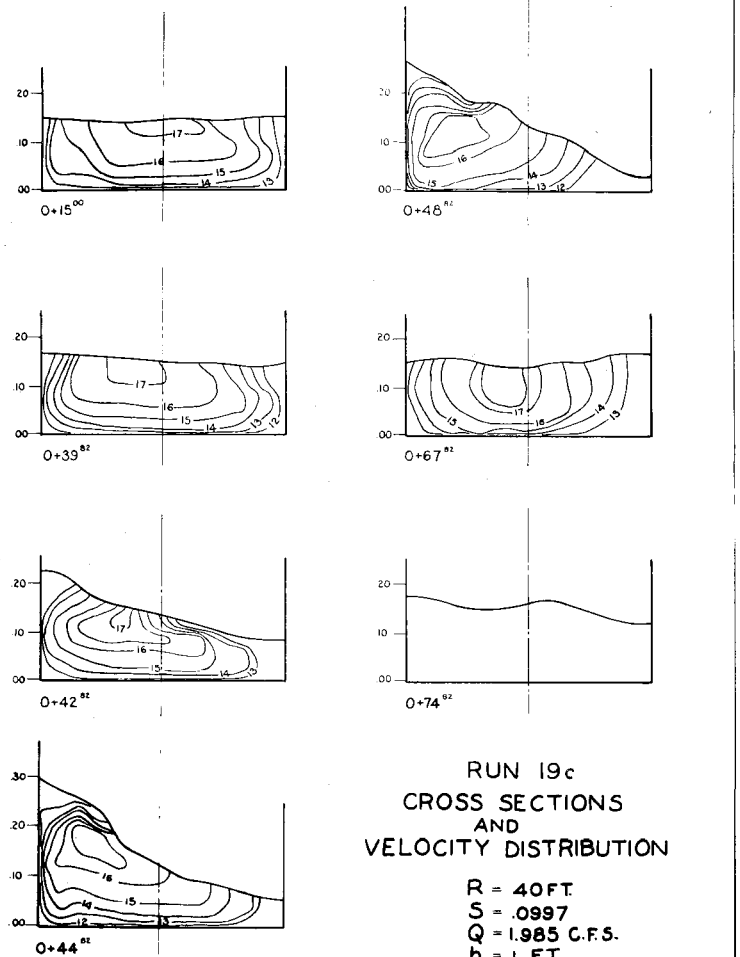
0+15.00
0+48.82
0+39.82
0+67.82
0+42.82
0+74.82
0+44.82
RUN 19c
CROSS SECTIONS
AND
VELOCITY DISTRIBUTION
R = 40 FT.
S = .0997
Q = 1.985 C.F.S.
b = 1 FT.

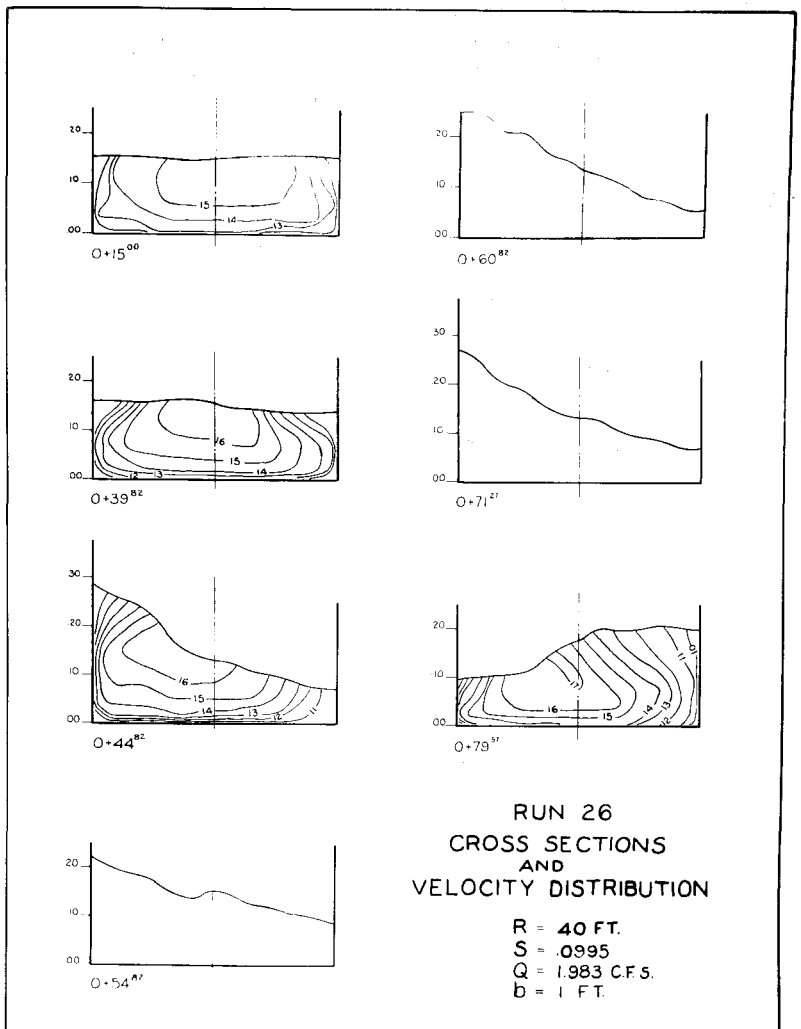
0+15.00
0+60.82
0+39.82
0+71.27
0+44.82
0+79.57
0+54.87
RUN 26
CROSS SECTIONS
AND
VELOCITY DISTRIBUTION
R = 40 FT.
S = .0995
Q = 1.983 C.F.S.
b = 1 FT.

Figure 19

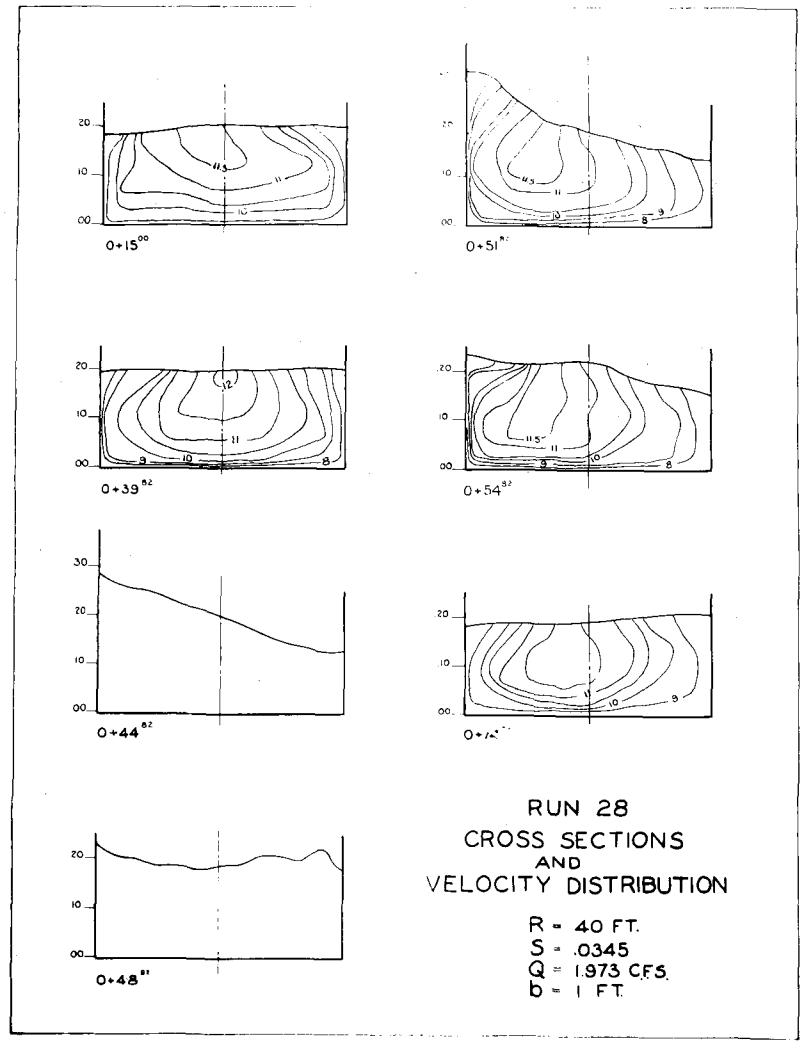
0+15.00
0+51.82
0+39.82
0+54.82
0+44.82
0+48.81
RUN 28
CROSS SECTIONS
AND
VELOCITY DISTRIBUTION
R = 40 FT.
S = .0345
Q = 1.973 C.F.S.
b = 1 FT.

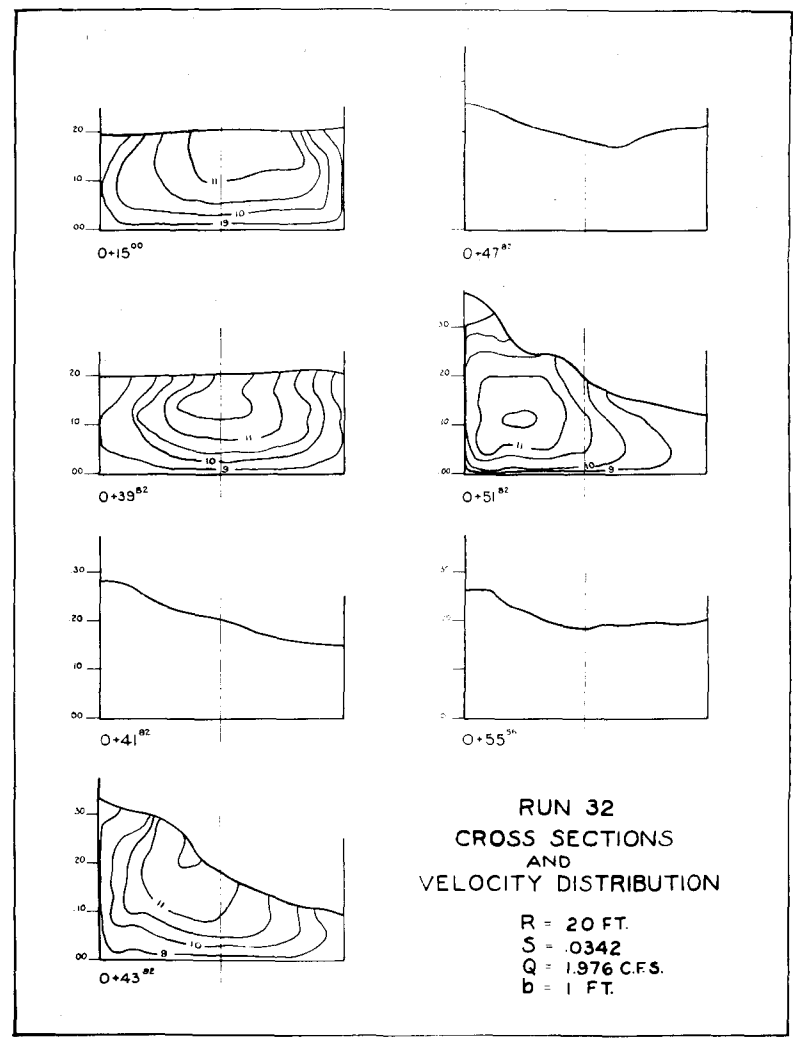
0+15.00
0+47.82
0+39.82
0+51.82
0+41.82
0+55.54
0+43.82
RUN 32
CROSS SECTIONS
AND
VELOCITY DISTRIBUTION
R = 20 FT.
S = .0342
Q = 1.976 C.F.S.
b = 1 FT.

Figure 20

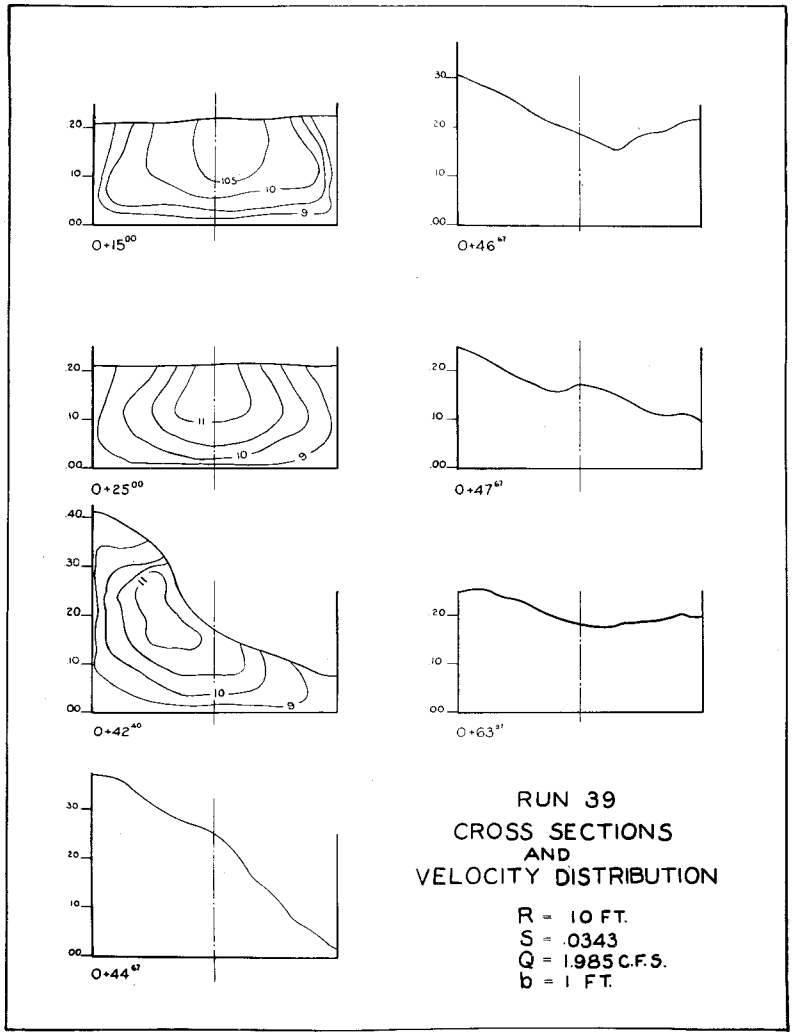
0+15.00
0+46.67
0+25.00
0+47.67
0+42.40
0+63.37
0+44.67
RUN 39
CROSS SECTIONS
AND
VELOCITY DISTRIBUTION
R = 10 FT.
S = .0343
Q = 1.985 C.F.S.
b = 1 FT.

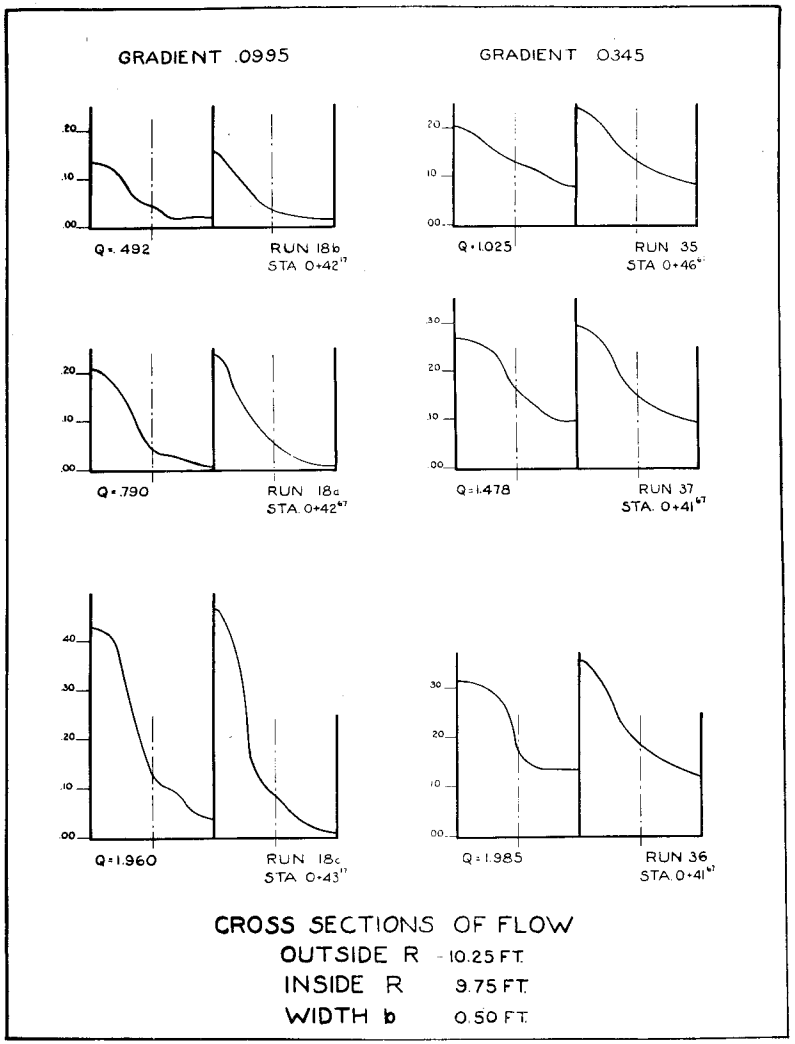
GRADIENT .0995
GRADIENT .0345
Q=.492
RUN 18b
STA 0+42.17
Q=1.025
RUN 35
STA 0+46.67
Q=.790
RUN 18a
STA 0+42.67
Q=1.478
RUN 37
STA. 0+41.67
Q=1.960
RUN 18c
STA 0+43.17
Q=1.985
RUN 36
STA 0+41.67
CROSS SECTIONS OF FLOW
OUTSIDE R 10.25 FT.
INSIDE R 9.75 FT.
WIDTH b 0.50 FT.

Figure 21

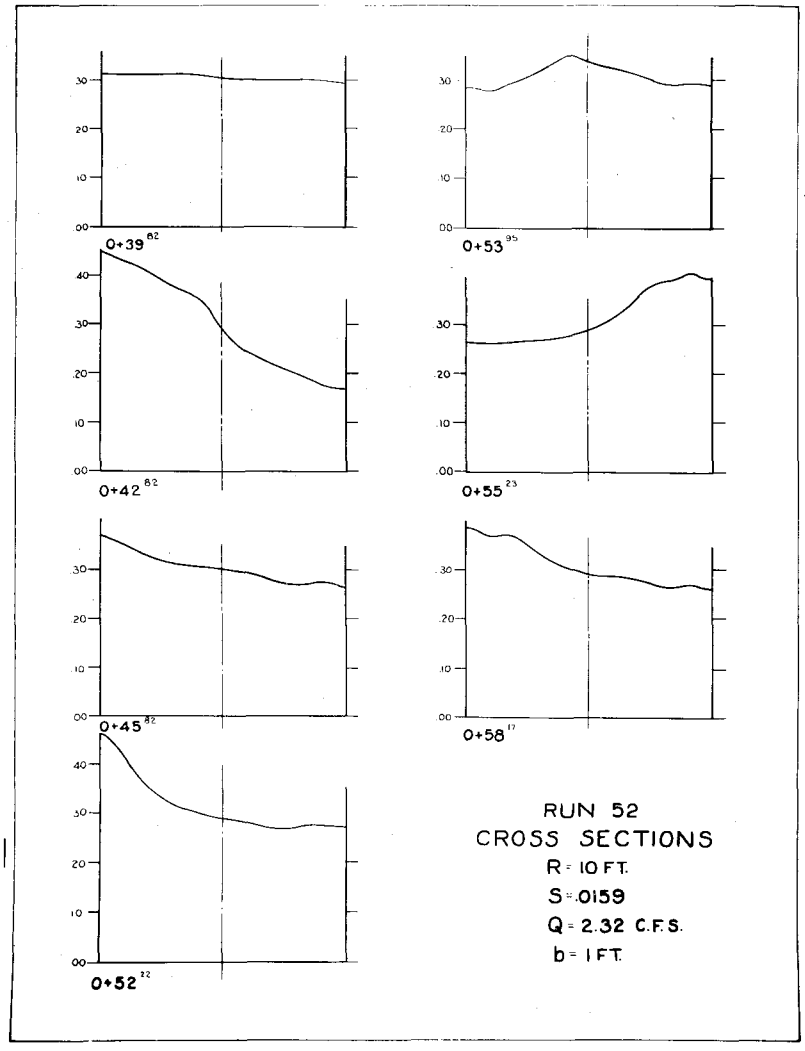
0+39 82
0+53 95
0+42 82
0+55 23
0+45 82
0+58 17
0+52 22
RUN 52
CROSS SECTIONS
R = 10 FT.
S = .0159
Q = 2.32 C.F.S.
b = 1 FT.

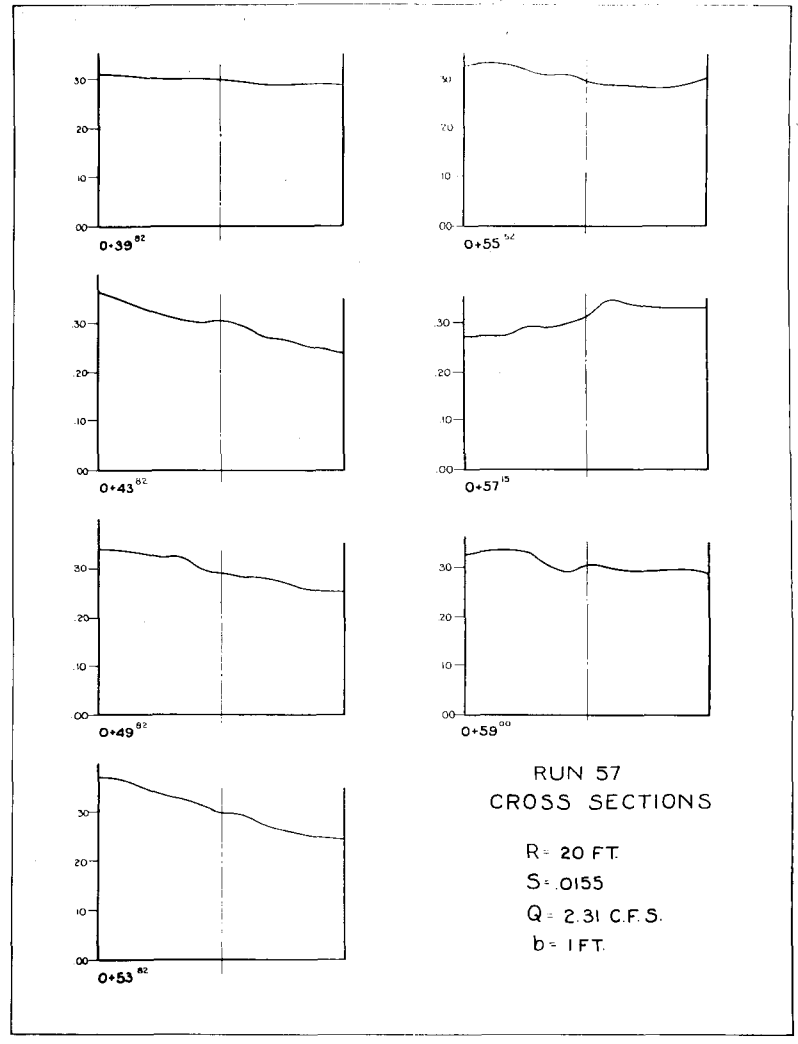
0+39 82
0+55 52
0+43 82
0+57 15
0+49 82
0+59 00
0+53 82
RUN 57
CROSS SECTIONS
R = 20 FT.
S = .0155
Q = 2.31 C.F.S.
b = 1 FT.

Figure 22

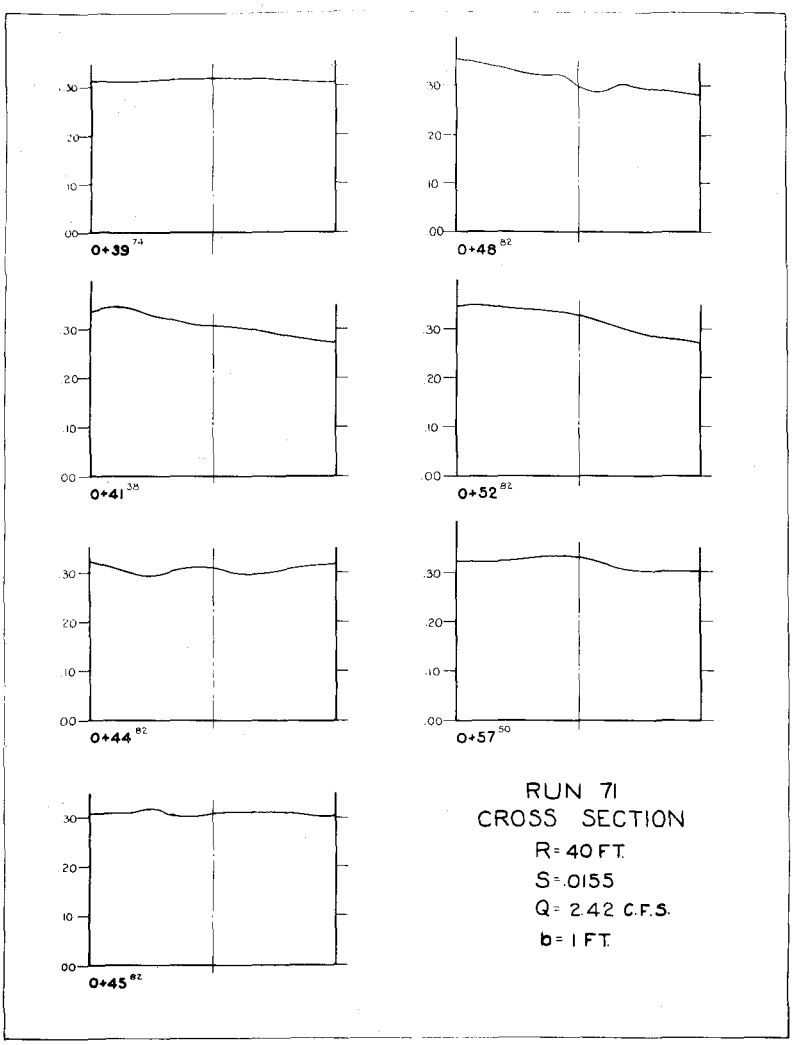
.30
.20
.10
.00
0+39 74
0+48 82
0+41 38
0+52 82
0+44 82
0+57 50
0+45 62
RUN 71
CROSS SECTION
R = 40 FT.
S = .0155
Q = 2.42 C.F.S.
b = 1 FT.

Figure 23

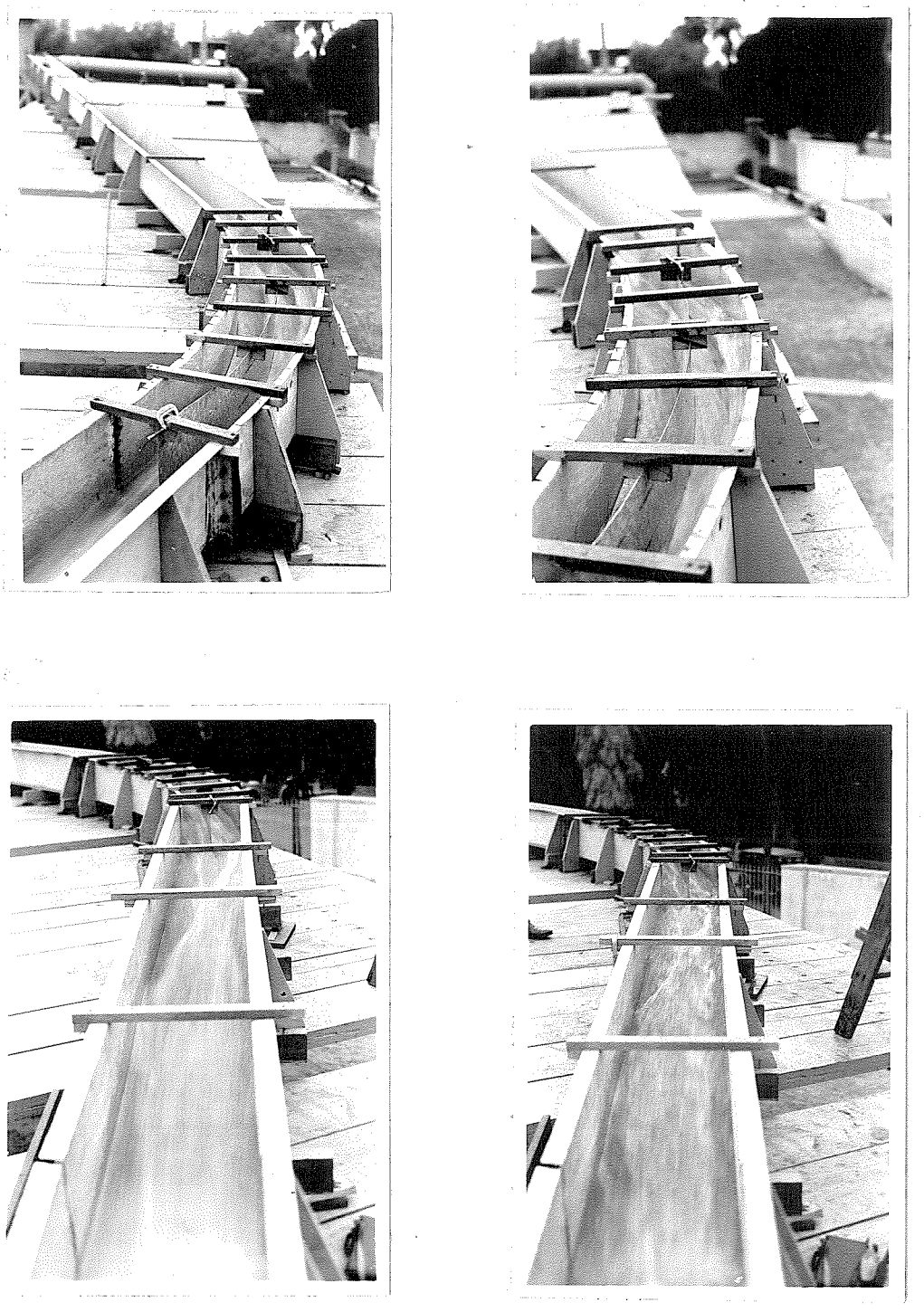

Figure 24

Run 18c, 10 foot radius, 45°.
Width divided in curved section to half.
Gradient .0995, Discharge 1.96 c.f.s.

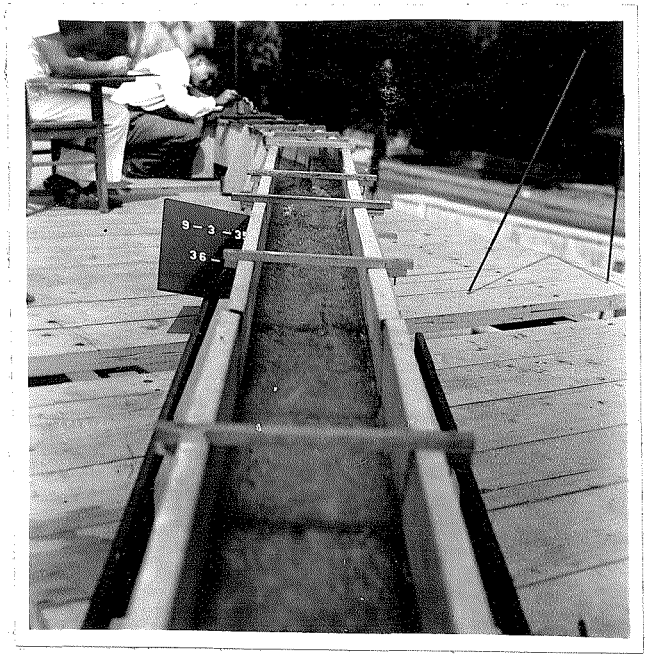

a. Looking upstream into straight section below curve.

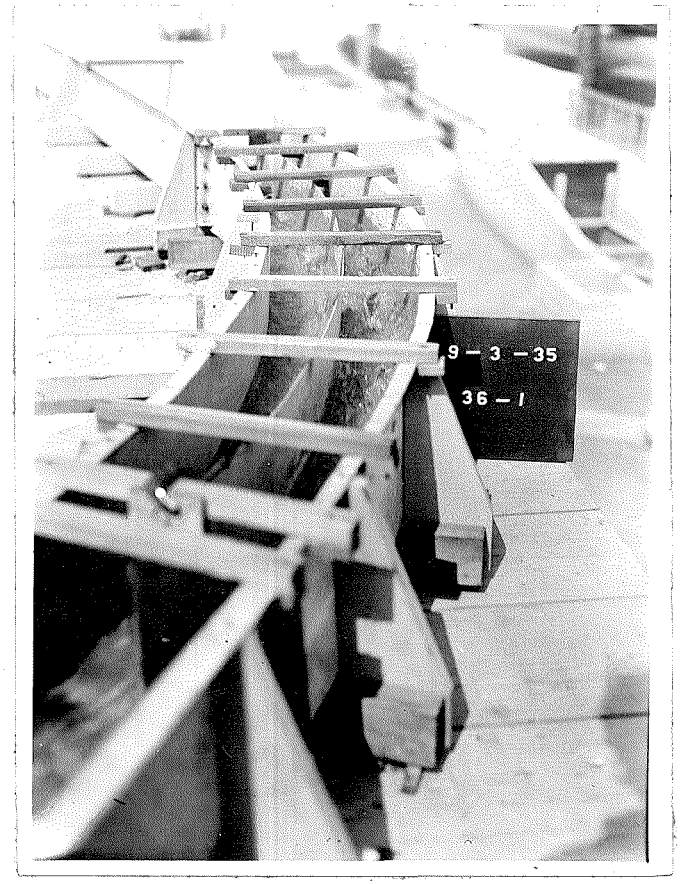

b. General view of curve divided into 2 channels.

c. Looking downstream into curve.

Figure 25 Runs 35 - 36, 10 foot radius, 45°. Gradient .0343, Discharges 1.025 c.f.s. and 1.985 c.f.s. respectively.

D. COMPARISON OF EXPERIMENTAL AND ANALYTICAL RESULTS

I. Comparison of Analytical and Experimental Profile of Rise.

Three relations were obtained in part B for the change in depth corresponding to a change in the direction of flow. These can be used to determine the profile of the water surface along the walls of a curved channel. The first two, equations 7 and 8, are respectively the approximate and exact forms derived on the basis of constant energy. Equation 12 is the exact equation obtained from the assumption of constant velocity. Table 2 shows a comparison of the values obtained with these three equations as compared to the measured results, of which we saw the plotted profiles under C. The runs presented in the following table were chosen to cover the entire range of the experimental program.

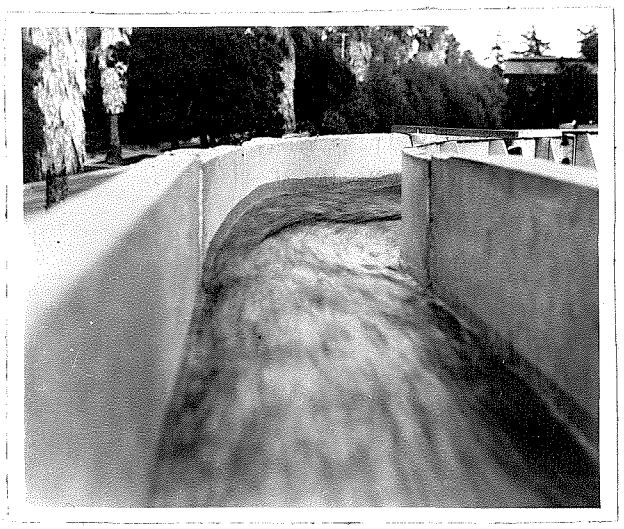

Figure 26

Figure 26 shows the appearance of the profile along the outer wall of the curve looking downstream into the curve. It

TABLE 2.

Run No.	Station	Slope Radius Discharge	Central Angle Θ radians	Measured Depth d feet	Constant Energy d(equ.7) feet	Constant Energy d(equ.8) feet	Constant Velocity d(equ.12) feet
3	39.82	.0995	0	.150	.150	.150	.150
	40.82	20'	.05	.205	.201	.203	.198
	41.82	1.988	.10	.253	.257	.258	.252
	42.82		.15	.310	.321	.318	.313
	43.65		.191	.349	.379	.364	.364
	43.82		.20	.363			
	44.82		.25	.419			
	45.82		.30	.445			
11	39.82	.0995	0	.111	.111	.111	.111
	40.67	10'	.085	.190	.183	.183	.176
	41.67	1.380	.185	.288	.293	.289	.278
	42.67		.285	.392	.429	.417	.399
	42.96		.314	.411	.470	.458	.445
	43.67		.385	.485			
	44.67		.485	.528			
15	39.82	.0995	0	.091	.091	.091	.091
	40.67	10'	.085	.143	.149	.148	.148
	41.67	1.015	.185	.231	.236	.233	.233
	42.67		.285	.321	.346	.337	.334
	42.93		.311	.350	.380	.372	.363
	43.67		.385	.407			
	44.67		.485	.412			
26	39.82	.0995	0	.146	.146	.146	.146
	40.82	40'	.025	.170	.171	.171	.170
	41.82	1.983	.050	.185	.196	.198	.195
	42.82		.075	.216	.223	.223	.222
	43.82		.100	.267	.254	.253	.252
	44.10		.107	.274	.262	.263	.260
	44.82		.125	.280			
28	39.82	.0345	0	.200	.200	.200	.200
	40.82	40'	.025	.207	.221	.218	.219
	41.82	1.973	.050	.227	.244	.240	.240
	42.82		.075	.257	.266	.263	.261
	43.18		.084	.268	.275	.272	.270
	43.82		.100	.280			

TABLE 2 (cont.)

Run No.	Station	Slope Radius Discharge	Central Angle Θ radians	Measured Depth d feet	Constant Energy d(equ.7) feet	Constant Energy d(equ.8) feet	Constant Velocity d(equ.12) feet
29	39.82	.0345	0	.164	.164	.164	.164
	40.82	40'	.025	.173	.182	.177	.179
	41.82	1.50	.050	.189	.201	.199	.196
	42.82		.075	.215	.221	.218	.213
	43.28		.086	.225	.229	.227	.223
	43.82		.100	.233			
32	39.82	.0345	0	.202	.202	.202	.202
	40.82	20'	.05	.226	.245	.244	.241
	41.82	1.976	.10	.285	.293	.290	.284
	42.74		.146	.320	.340	.335	.325
	42.82		.15	.323			
	43.82		.20	.329			
39	39.82	.0345	0	.212	.212	.212	.212
	40.67	10'	.085	.277	.290	.286	.278
	41.67	1.980	.185	.365	.392	.382	.366
	42.15		.233	.393	.444	.443	.415
	42.67		.285	.426			
	43.67		.385	.429			
55	39.82	.0145	0	.284	.284	.284	.284
	40.82	10'	.10	.351	.372	.366	.353
	41.63	2.145	.181	.388	.450	.443	.410
	41.82		.200	.394			
	42.37		.255	.415			
62	39.82	.0145	0	.273	.273	.273	.273
	40.82	20'	.05	.301	.313	.310	.304
	41.79	1.995	.098	.314	.355	.349	.337
	41.82		.100	.318			
	42.82		.150	.331			

will be seen that the measured and the calculated values of depth are in very good agreement. The three equations give very similar results. However equation 12 (constant velocity) appears to give values consistently closer to the observed points than do equations 7 and 8. Equations 7 and 8 differ hardly at all from each other within the range of practical applications. On the basis of simplicity and of closeness of agreement equation 12 is to be recommended.

All three equations are applicable also to the profile along the inside wall and in this case give the fall. For example, when used for the inside wall profile equation 12 becomes

$$(12a) \qquad d = \frac{v^2}{g} \sin^2\left(\beta_o - \frac{\theta}{2}\right)$$

θ has the negative sign because the wall is turning away from the flow.

II. Comparison of Analytical and Experimental Maxima

Table 3 presents a comparison of the values of the maxima calculated from the same three equations and the experimental values. All of the runs made with simple curves are presented in this table. It will be noted that in several cases there are two sets of readings given for a single run number. In every case the second set refers to conditions in the return curve. Although at the time this second curve was not considered as a part of the test section it will be seen that the agreement between the analytical and experimental values is very good.

TABLE 3.

Run	Depth d_o feet	Central Angle Θ_o	Measured h' feet	For Constant Energy h'(equ.7) feet	For Constant Energy h'(equ.8) feet	Constant Velocity h'(equ.12) feet
1	.096	11°04'	.281	.246	.243	.237
2	.123	11°20'	.377	.326	.323	.313
3	.150	10°58'	.445	.379	.374	.364
4	.137	11°23'	.427	.366	.367	.360
5	.118	11°29'	.351	.326	.320	.313
6	.091	11°05'	.257	.237	.234	.228
7	.055	11°34'	.145	.156	.155	.151
8	.103	11°45'	.325	.300	.303	.294
9	.070	11°43'	.200	.202	.197	.196
11	.111	18°02'	.528	.470	.458	.445
12	.147	17°42'	.746	.612	.594	.569
13	.144	17°49'	.764	.601	.585	.575
14	.124	18°16'	.638	.557	.545	.525
15	.091	17°49'	.412	.380	.372	.363
16	.061	17°38'	.242	.243	.237	.231
17	.048	17°03'	.176	.169	.155	.145
18a	.0813	11°02'	.207	.214	.211	.207
18a	.0795	11°17'	.232	.212	.211	.206
18b	.062	10°31'	.134	.146	.145	.141
18b	.059	11°00'	.151	.149	.146	.146
18c	.152	10°38'	.389	.349	.367	.359
18c	.145	11°02'	.450	.333	.365	.358
19c	.146	6°06'	.296	.267	.261	.259
20	.134	6°35'	.260	.249	.247	.242
21	.111	6°31'	.230	.212	.215	.207
22	.089	6°19'	.188	.167	.168	.165
23	.076	6°19'	.155	.140	.140	.138
24	.078	6°23'	.151	.141	.141	.138
25	.136	6°23'	.244	.247	.244	.241
26	.146	6°08'	.280	.263	.262	.260
28	.200	4°47'	.280	.275	.272	.270
29	.164	4°57'	.233	.229	.227	.223
30	.123	4°43'	.170	.168	.168	.165
30a	.180	8°18'	.274	.295	.293	.283
32	.202	8°22'	.329	.340	.335	.325
33	.128	8°32'	.206	.219	.216	.209
34	.105	8°40'	.165	.183	.177	.173
35	.138	7°31'	.191	.218	.213	.218
35	.136	8°04'	.234	.219	.217	.210
36	.211	7°47'	.317	.337	.332	.321

TABLE 3 (cont.)

Run	Depth d_o feet	Central Angle Θ_o	Measured h' feet	For Constant Energy h'(equ.7) feet	For Constant Energy h'(equ.8) feet	Constant Velocity h'(equ.12) feet
36	.212	8° 08'	.354	.343	.339	.329
37	.166	8° 16'	.267	.279	.283	.272
37	.163	8° 40'	.290	.281	.276	.270
38	.109	13° 52'	.226	.241	.233	.222
39	.212	13° 25'	.429	.444	.443	.415
41	.140	14° 18'	.318	.326	.316	.301
42	.169	13° 56'	.383	.377	.367	.350
43	.140	14° 00'	.296	.313	.308	.293
44	.156	14° 2 '	.345	.379	.353	.336
45	.184	13° 49'	.396	.406	.408	.377
46	.208	13° 39'	.454	.447	.440	.409
47	.207	13° 42'	.462	.449	.441	.416
48	.218	10° 24'	.324	.348	.340	.319
49	.166	10° 32'	.255	.267	.262	.244
49	.166	6° 07'	.210	.222	.219	.212
50	.196	10° 13'	.296	.307	.301	.279
50	.196	5° 41'	.253	.255	.252	.240
51	.243	10° 25'	.369	.385	.378	.352
51	.243	5° 46'	.339	.319	.314	.302
52a	.304	10° 18'	.440	.481	.469	.438
52a	.304	5° 46'	.449	.398	.394	.377
52	.302	10° 24'	.447	.478	.466	.437
52	.302	5° 45'	.432	.394	.389	.375
53	.107	10° 27'	.155	.171	.170	.156
54	.302	10° 11'	.451	.480	.471	.431
55	.284	10° 22'	.415	.450	.443	.410
56	.137	10° 35'	.214	.221	.217	.202
57a	.299	5° 45'	.385	.391	.386	.373
57	.298	5° 45'	.360	.391	.387	.372
57	.298	10° 28'	.444	.473	.465	.433
58	.299	5° 46'	.357	.391	.386	.371
58	.299	10° 26'	.437	.473	.464	.433
59	.227	6° 08'	.266	.302	.299	.289
59	.227	9° 50'	.329	.356	.347	.327
60	.146	6° 05'	.186	.193	.192	.185
60	.146	10° 28'	.214	.234	.229	.214
61	.197	6° 03'	.237	.260	.260	.249
61	.197	10° 34'	.272	.317	.311	.289
62	.273	5° 38'	.331	.355	.349	.337
63	.307	5° 31'	.373	.393	.390	.374
63	.307	9° 59'	.423	.470	.464	.432
64	.146	5° 58'	.183	.192	.192	.183

TABLE 3 (cont.)

Run	Depth d_o feet	Central Angle Θ_o	Measured h' feet	For Constant Energy h'(equ.7) feet	For Constant Energy h'(equ.8) feet	Constant Velocity h'(equ.12) feet
65	.240	5°48'	.287	.312	.312	.296
66	.260	2°48'	.290	.298	.297	.293
67	.196	3°21'	.231	.240	.231	.226
68	.141	2°59'	.154	.162	.161	.157
69	.189	2°36'	.208	.213	.210	.209
70	.240	3°03'	.272	.278	.276	.269
71	.312	2°59'	.351	.360	.356	.350
72	.301	2°59'	.381	.345	.343	.337
73	.285	3°21'	.320	.318	.318	.316
74	.250	2°48'	.288	.286	.283	.277
75	.202	3°06'	.234	.235	.235	.228
76	.172	2°44'	.199	.196	.195	.191
77	.144	2°59'	.171	.166	.165	.161

An inspection of the table shows that only in the cases of extremely high superelevation is there a bad agreement between the observed and calculated values. Figure 12 shows the appearance of this class, where perhaps 50% of the channel floor is exposed in the curve. Such cases would be avoided in design because of the excessive wall height demanded. Their occurrence is to be expected when the calculated height is more than three times the average depth at entrance. The reason for this discrepancy between calculation and observation is found in the determination of θ_o. The simplified formula proposed for finding the point of first maximum assumes that the interfering wave travels on a stream of constant depth with parallel flow. In the normal case the deviations in depth are roughly compensated by a simultaneous change of angle of flow. This compensation is not satisfactory for extremely high deviations in depth from that of the entering value. In such cases the change in the angle of flow has the predominating influence with the result that the point of maximum depth is shifted downstream. If θ_o is corrected for this shift then the maximum calculated depth will agree with the observations. Since the practical value of such cases is very small it has been felt unwise to introduce the additional complications required for this correction.

The above discussion also explains the fact that in Table 2 the calculated columns do not always extend down to the point of the observed maximum.

It is pertinent at this point to add a rough calculation to show that for cases of small curvature the maximum outside depth in

the beginning of a curve can be related to the old formula for superelevation $h = \frac{v^2 b}{Rg}$ in the following way:

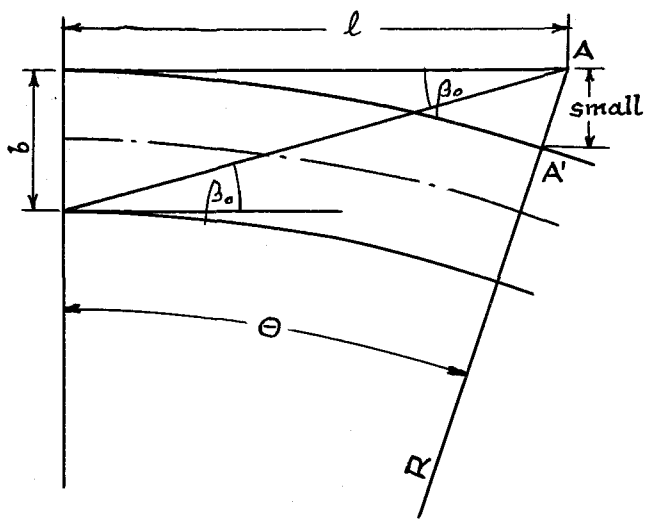

Figure 27

According to $h = \frac{v^2 b}{Rg}$ the maximum outside depth would be $d_o + \frac{v^2 b}{2Rg} = h'$ for velocities lower than the critical. By the following approximation it can be shown that for supercritical flow the change of depth from d_o to d_{max} should be twice that for lower than critical flow:

$$h' - d_o = 2\,\frac{v^2 b}{2Rg} = \Delta d$$

Assuming a small curvature, so that AA' becomes negligible,

$$\Delta d = \frac{v^2}{g} \tan\beta_o \cdot \Theta$$

since $\Theta \approx \frac{\ell}{R}$

$$\tan\beta_o = \frac{b}{\ell}$$

$$\Delta d = \frac{v^2}{g} \cdot \frac{\ell}{R} \cdot \frac{b}{\ell} = \frac{v^2 b}{Rg}$$

This shows that for supercritical velocities the increase in depth is twice that for subcritical ones, if we consider only very small curvatures.

III. The General Pattern of Disturbances Set Up by Curves

The wave pattern set up by the curves when the flow is in the field of supercritical velocity is very definite and striking.

Figure 28 shows the wave crest diagrams for all of the runs in the original schedule.

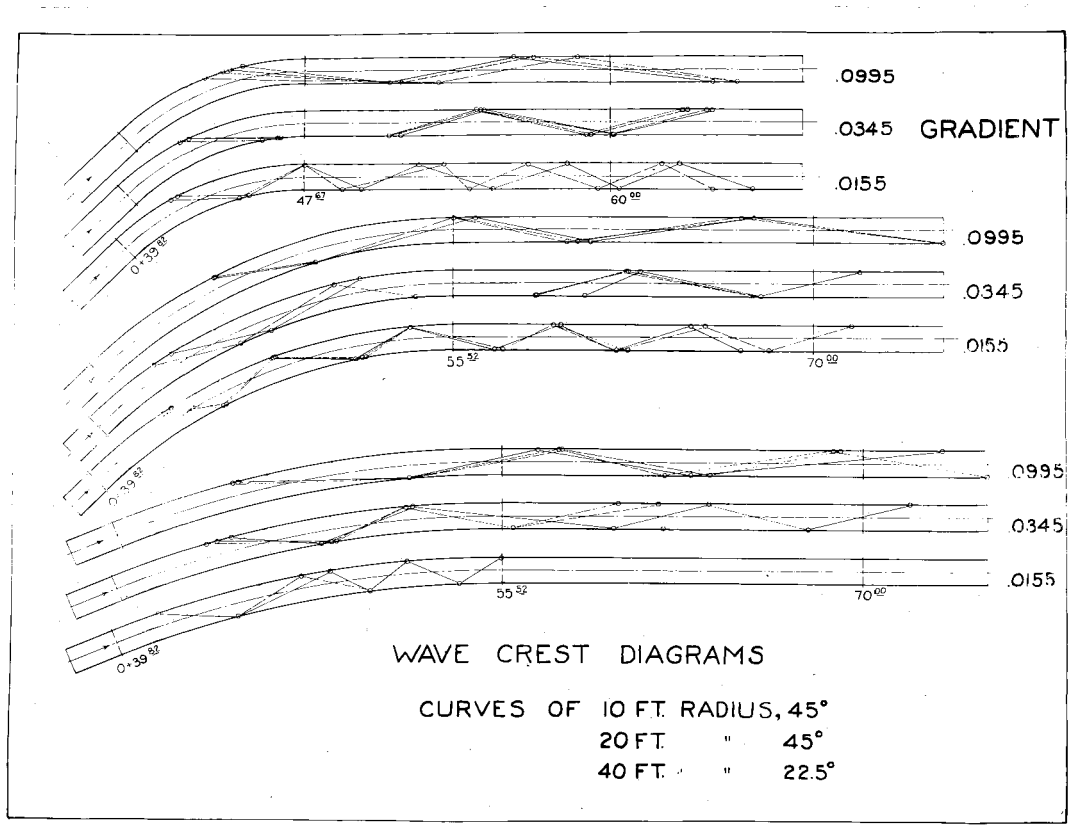

Figure 28

(a) Constancy of Pattern for Given Channel

One of the first points to be observed in this series of diagrams is the remarkable similarity of pattern for the different runs in a given curve, channel, and gradient. This is the condition represented by the individual diagrams. The reason for this agreement is simple. The channel velocity varies roughly with the square root of the mean depth. The wave velocity also varies with the square root of the depth. Therefore the wave angle, being the ratio of the two, remains a constant. The reason

that this is not exactly adhered to in the experimental results is because neither the channel velocity nor the wave velocity are affected by the average depth alone. The channel velocity is modified by the width-depth ratio, while the wave velocity is modified by the rise itself. One useful conclusion that comes out of this similarity is that the points of maxima, both in the curve and in the downstream tangent, will remain at the same location independent of the rate of discharge for all cases above a small rate of flow.

(b) Spacing of Maxima

The next point of interest is the spacing of the successive maxima. Considering a single diagram it is seen that the spacing is quite uniform. Comparing channels of the same gradient but with curved sections of different radius, it is observed that the spacing in the downstream tangent is not affected by the change in curvature. For small disturbances this spacing can be calculated by taking 2 times $\frac{b}{\tan \beta_o}$, where β_o is the wave angle calculated from the initial depth and velocity above the curve. The spacings have been calculated on this basis and compared to the experimental ones. It was found that $2\frac{b}{\tan \beta_o}$ gives a good average value, within $\pm 10\%$. Since, however, the data are not sufficiently complete to allow a definite statement the table giving the calculated and the experimental spacings was not included here.

(c) Number of Maxima in Curve

It follows from the above that maxima will be spaced in the curve in somewhat the same manner as in the downstream tangent. However the distances of travel are modified by the curvature. In the curve, as was seen before, the angle θ_o is the equivalent of

the factor $\frac{b}{\tan\beta_o}$ and is more convenient. Maxima are to be expected at θ_o, $3\theta_o$, $5\theta_o$, etc. If the central angle of the curve is less than θ_o, the full maximum depth will not be attained. In this case the central angle itself is used to determine the maximum depth. It can be stated also that the angle θ_o due to the method of its calculation represents a minimum angular distance to the point of maximum depth. This is shown clearly on Table 2, where the points of the measured maximum depths are seen to lie downstream from the calculated positions.

(d) Relative Height of Maxima in Downstream Tangent

Some general conclusions are possible concerning the relative depths of the disturbance in the straight channel below the curve. The magnitude of this downstream disturbance depends upon the angle at which the last wave crest from the curved portion enters the straight section. The less this angle, the less will be all of the downstream maxima. The minimum of this angle is 0 and the maximum is the true value of β at the last maximum in the curve. Thus it is seen that a fortuitous choice of central angle might result in a very small downstream disturbance. Such cases are seen for the 20 and 40 foot curves with 3-1/2% gradient as shown in Figures 9 and 10. On the other hand an unfortunate central angle can project the wave crest into the straight section with the full angle. In such cases the disturbance is of the same approximate magnitude as the last one in the curve. An example of this is shown in Figure 11, for the 10 and 20 foot radii on 1-1/2% slope. These considerations can also be expressed in the

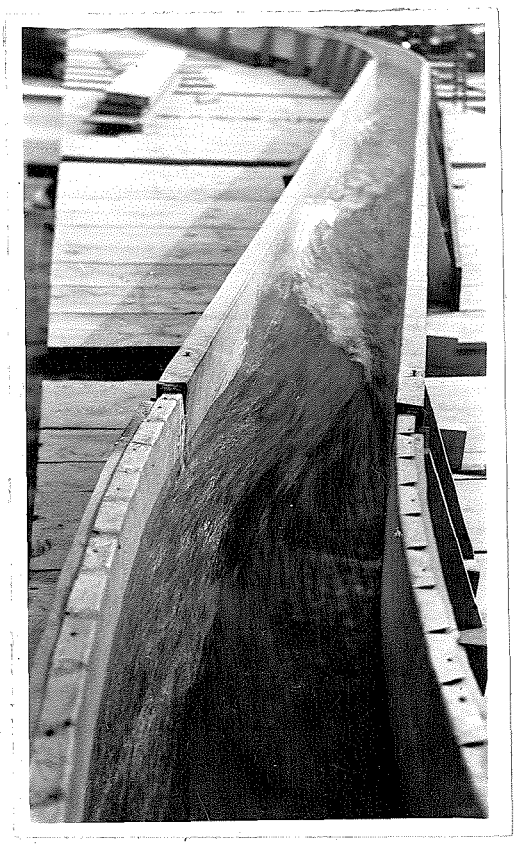

(a) Looking downstream.

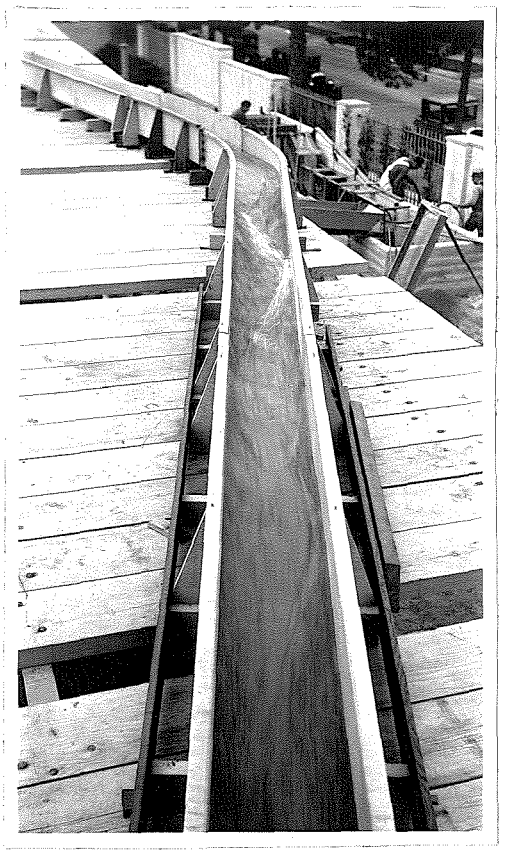

(b) Looking upstream.

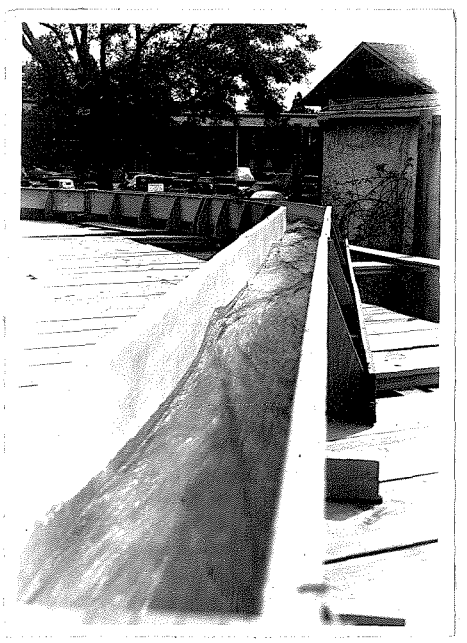

(c) Looking downstream.

Figure 29

(P)

form used in section (f) of the summary.

Figures 29 and 30 show a group of photographs of the wave patterns in the downstream section. Figure 29 (a) and (b) are for the same run, which was for a 10 foot radius curve, 2.3 cubic feet per second discharge and 3-1/2% slope. It will be observed in (a) that the last maximum occurs just at the end of the curve. The resulting high downstream disturbances are easily seen. The last photograph, (c), shows the appearance below a 20 foot radius curve for a very low discharge. Both (b) and (c) illustrate the persistence of the disturbance. Figure 30 shows the appearance of the run whose profile is shown in Figure 11. These are both for the 10 foot curve. The shorter wave lengths, typical of the low velocities, should be noted.

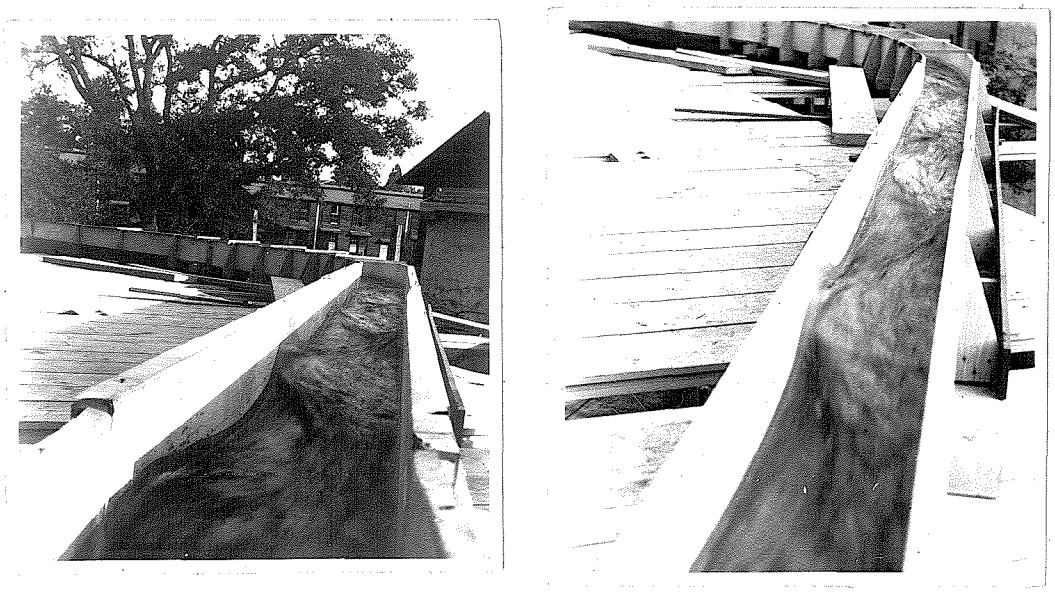

(a) Looking downstream. (b)

Figure 30

E. GENERAL DISCUSSION AND FINAL CONCLUSIONS

A study of the wave patterns and surface configurations obtained in the experimental investigation suggested possible methods of influencing either one by a change of the boundary conditions. It should be possible to reduce the maximum depth and to minimize the downstream disturbance by a suitable choice of the wall curvatures. An empirical attempt in this direction was made by the construction of compound curves. The purpose was to cut down the maximum disturbance by introducing the sharp curvature after the first maximum had started to subside. Some success in this direction, so far as the maximum in the curve was concerned, was achieved, as may be seen from the Figures 31 and 32. These Figures represent surface profiles along the channel walls and may be given here without much further discussion. They indicate however that there are interesting possibilities especially if the most suitable wall curvatures could be determined by a graphical step by step procedure.

A case of relative importance for practical design is that of a number of curves in succession. It can be seen from the graphs that the disturbances caused in the downstream tangents do not die out very rapidly. All the cases investigated experimentally and also the analytical discussion are based on the assumption that the flow entering the curved section is of uniform depth and with parallel streamlines. It is conceivable that with curves following each other in relatively short distances the disturbances may add up to a value much higher than that for the individual curve. This could

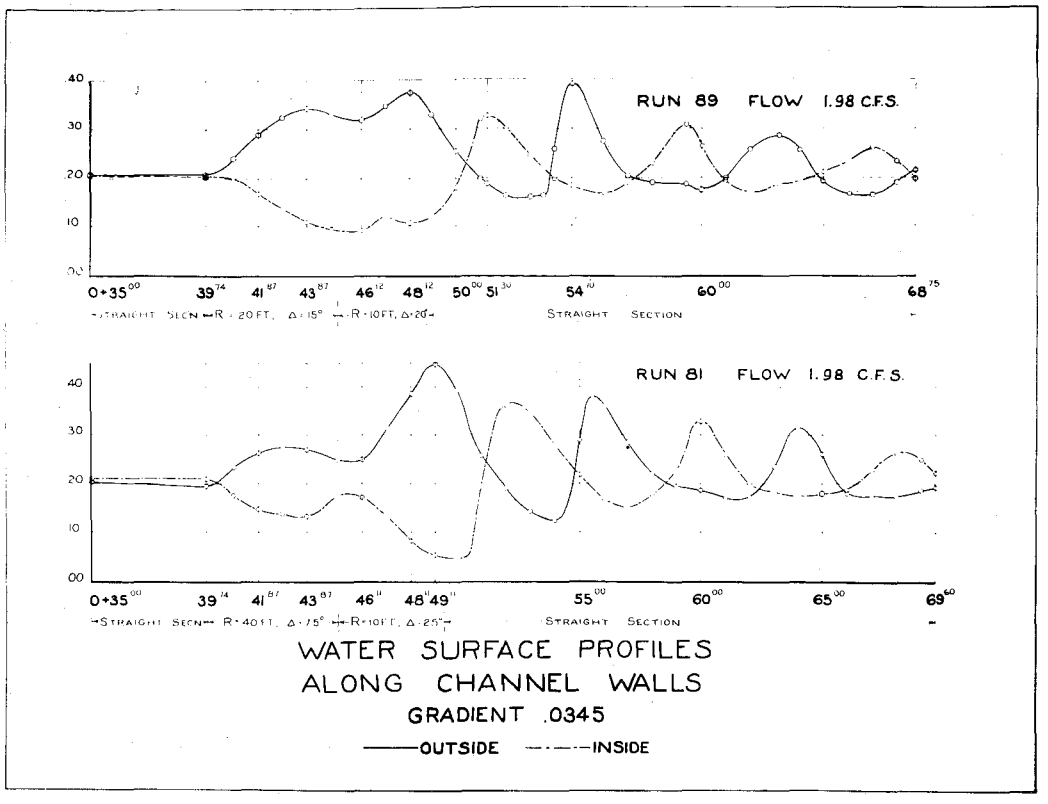
RUN 89 FLOW 1.98 C.F.S.
RUN 81 FLOW 1.98 C.F.S.
STRAIGHT SECTION
WATER SURFACE PROFILES
ALONG CHANNEL WALLS
GRADIENT .0345
OUTSIDE
INSIDE

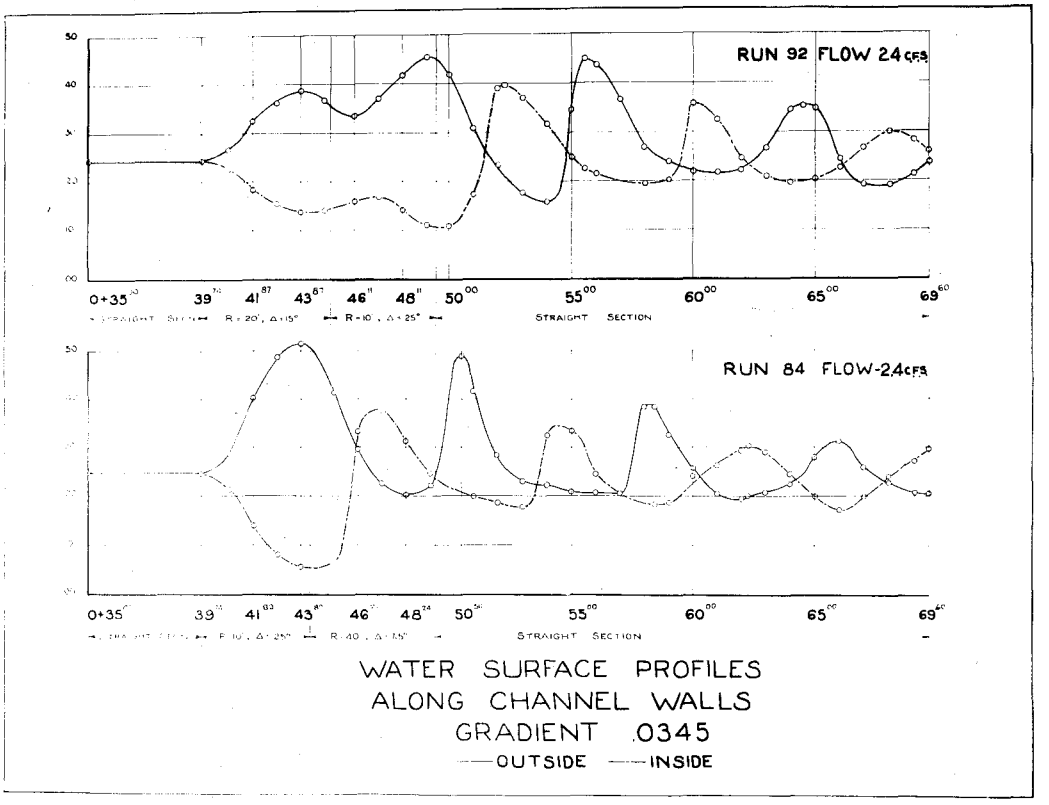
RUN 92 FLOW 2.4 C.F.S.
RUN 84 FLOW-2.4 C.F.S.
STRAIGHT SECTION
WATER SURFACE PROFILES
ALONG CHANNEL WALLS
GRADIENT .0345
OUTSIDE
INSIDE

Figure 31

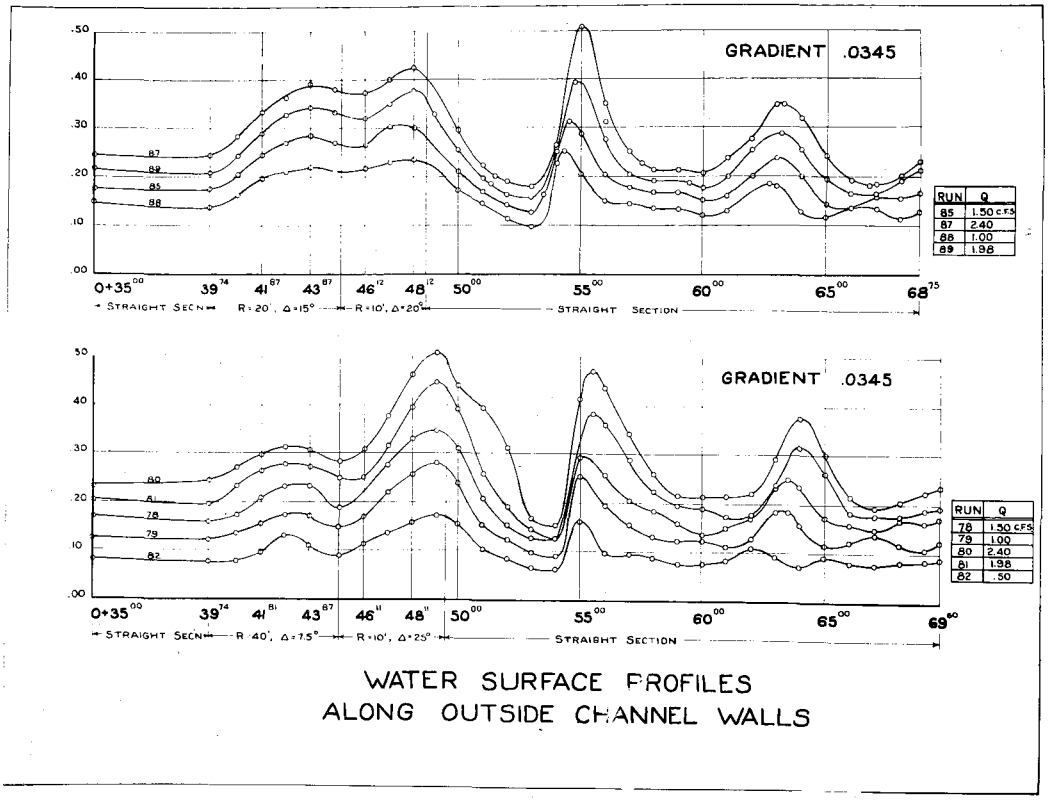

WATER SURFACE PROFILES
ALONG OUTSIDE CHANNEL WALLS

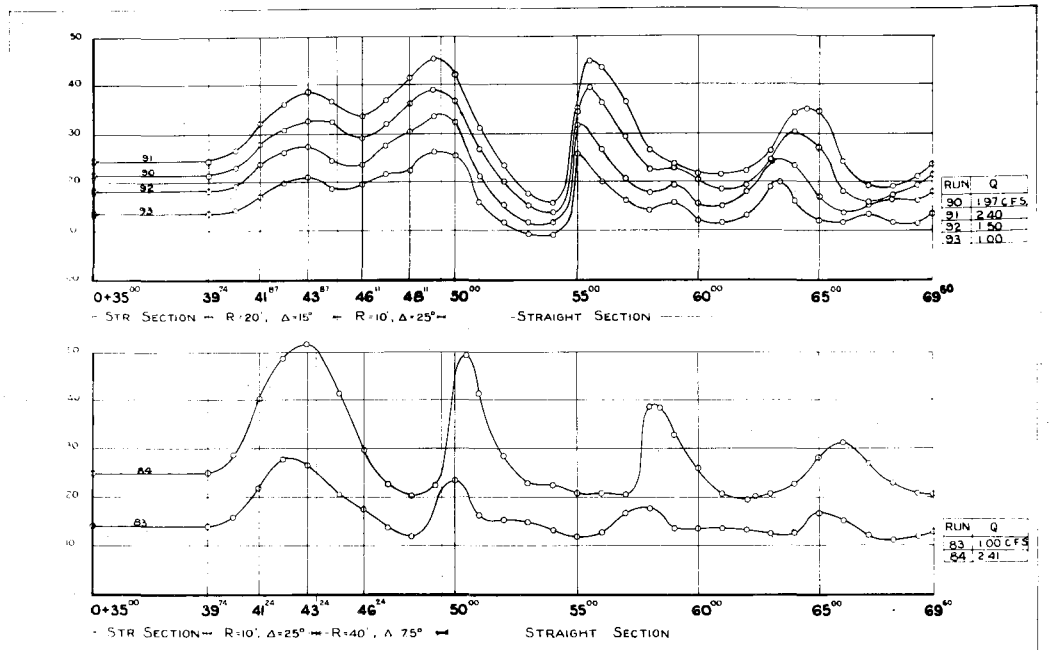

WATER SURFACE PROFILES
ALONG OUTSIDE CHANNEL WALLS
GRADIENT .0345

Figure 32

be properly termed a case of resonance. Cases of damping are just as probable however.

A final answer to these involved problems with the present state of knowledge could only be given by a model study.

Another question can be answered more definitely. From the derivations of the analytical expressions it is seen that the density does not appear. It follows that entrained air or debris in suspension do not affect the validity of the derived equations. They enter only insofar as they influence the conditions of flow, i.e. the relations between depth and velocity.

It is believed that with this analytical and experimental study the understanding of high velocity flow phenomena has ben furthered a great deal and that the way to satisfactory solutions of the numerous problems facing the engineer in this field has been opened.

APPENDIX I

The Experimental Set-Up for Studies of High Velocity Flow. - The Circulation System

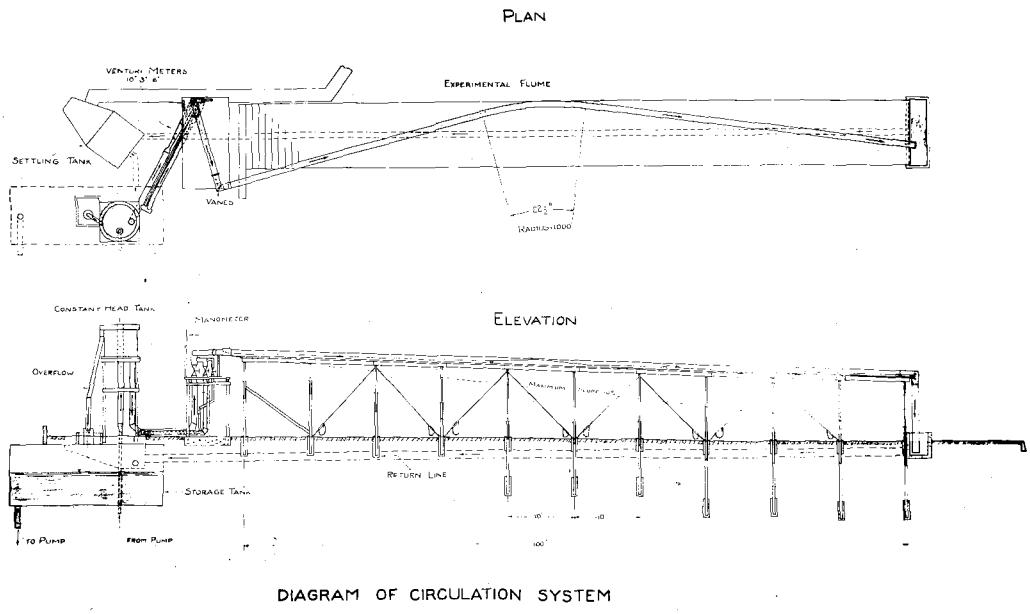

DIAGRAM OF CIRCULATION SYSTEM

Figure 33

Corresponding to the analysis of conditions and variables to be represented the experimental set-up was designed and constructed as shown schematically in Figure 33.

The detailed dimensions of the set-up are given in the added plan, Figure 34.

A closed circuit is provided for the flow. The water is drawn from a storage-reservoir of about 1400 cu. ft. capacity and is lifted by a centrifugal pump to the constant head tank of 6 ft.

PLAN

NOTE:
⊕ These Points mark ground elevations of graded surface.

(Concrete Flume)

Earth ramp

East Wall of Model Basin

8" pipe to west side of Model Basin

6" pipe from pump

Building Line

Mech. Engg Laboratory 135'-6"

Concrete Curb

LONGITUDINAL SECTION

Total length of trestle 101'-6"

Max. Slope 1:10

Ground Slope 1:100 Approx.

Return Line - 12" concrete pipe Approx. Slope 1:300

CALIFORNIA INSTITUTE OF TECHNOLOGY HYDRAULIC STRUCTURES LABORATORY		
FLOOD WAVE INVESTIGATION GENERAL LAY-OUT OF 100 FT. FLUME		
SCALE 1" = 5'	DRAWN: A.T.I.	DATE: 5-2-'35
	CHECKED: A.T.I.	DRWG: NO. F 1

diameter and 5 ft. depth. The maximum obtainable discharge is around 2.5 cu. ft. per sec. The water flowing through the experimental flume is taken from the constant head tank through a 10" pipe to the upper end of the flume. On its way it passes through either a 10", 6" or 3" Venturi meter, by which the discharge is measured. The surplus water pumped to the constant head tank is wasted over the crest and led back directly to the storage reservoir below. In this way a constant supply to the test-flume is assured. The water is released into the flume through a rectangular nozzle at a velocity adjusted to the velocity of uniform flow in the flume for the given hydraulic conditions. At the end of the testing-flume the stream is diverted by vanes vertically into the collecting-basin and flows back through a concrete return line to the settling basin. An overflow discharges it from here to the storage tank.

(a) The Discharge Measurement

All the discharges were measured by specially constructed Venturi meters installed above the flume entrance. Three different sizes of Venturi's are installed in long parallel lines of 10", 6" and 3" diameter pipe. In this way for any discharge from the smallest to the largest possible the pressure-differences between throat-section and full cross-section can be read by means of a water-manometer with the same degree of accuracy

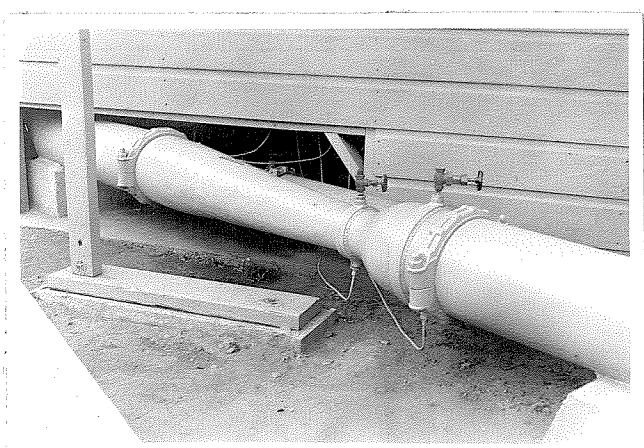

Figure 35 10" Venturi-Meter

throughout the range of discharges. These Venturi meters were calibrated accurately by diverting the discharge into a measuring tank and determing the volume of discharge over a considerable time. This was done with the Venturis in their final positions. Since the meters had been galvanized the calibration will not change with time.

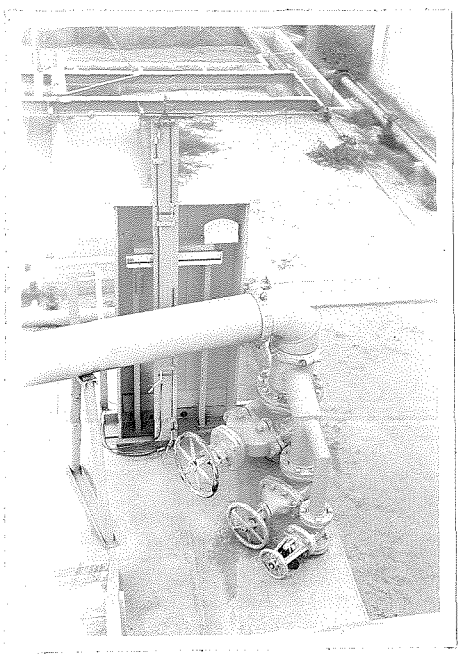

Figure 36

Venturi Manometer and Regulating Valves

The size of the measuring tank made it possible to keepthe time of discharge always above 30 seconds, thus minimizing any error from this side. The water-level of the filled tank did not change over a long period of time, which indicates that there was no leakage of any discernable amount. The height-gauge reading was taken after the water surface in the measuring tank had calmed down sufficiently to read the gauge within one-thousandth of a foot. Thus the total volume of water could always be determined to 1/10 of a cu. ft.

It can be stated in conclusion, that the calibration of the Venturi-meters permits easily the determination of the flow of water through the system within 1/2 to 1%. The variations of flow, as indicated by the manometer, were less than 1% for the en-

tire period of any run.

(b) The Tilting Platform

The platform is constructed in such a way that it can be adjusted to any slope between zero and 1:10 over the entire length of 100 ft. It is divided into 10 sections, which can be adjusted individually. It is, therefore, possible to obtain any form of a profile. By using the lower 6 sections only, the slope of these may even be adjusted to 1:5. This flexibility together with the available total drop of 11 ft. makes this structure especially suited to high-velocity investigations.

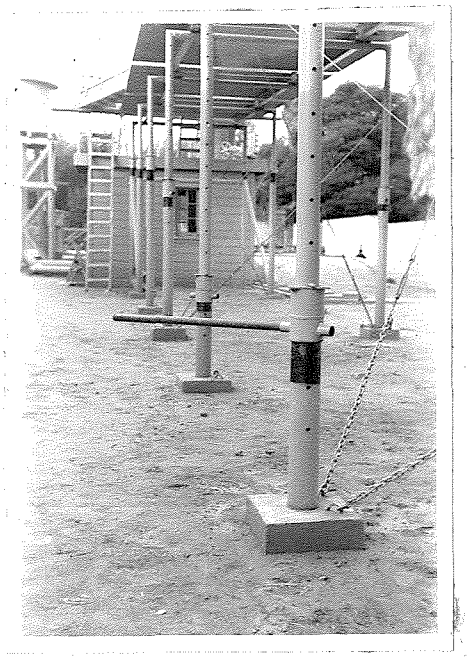

Figure 37

Slope Adjustment

The method for both coarse and fine adjustments of the slope is clearly seen from Figure 37, which also illustrates the cross-bracing that insures the rigidity of the platform.

(c) The Experimental Flume

The experimental flume was built of galvanized iron. The width was 12 inches. Since high super-elevations were to be expected, the depth was 10 inches, which is proportionally much higher than could be used economically in large channels.

The flow was released into the flume through a rectangular nozzle with an adjustable tongue, by which it was possible to regulate the velocity and the depth in the straight section of approach.

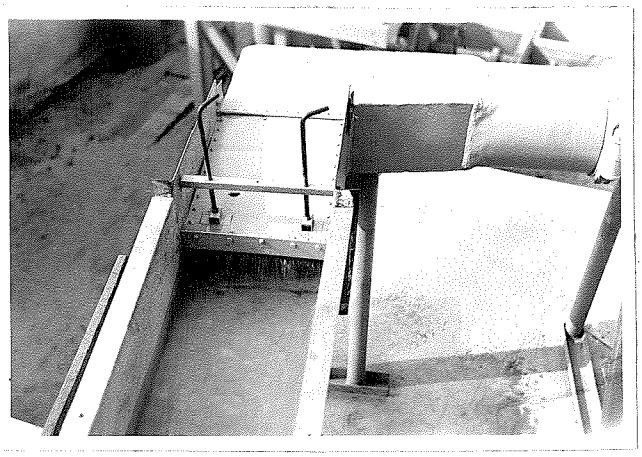

Figure 38 Entrance Nozzle

Curved sections were constructed for each of three different radii of curvature, i.e. 10, 20, and 40 ft. to the channel centerline. All sections were carefully reinforced to prevent their distortion due to their own weight or the weight of the water. Joints were made with flanges or with butt straps soldered to the outside so that no obstructions were introduced into the flow.

(d) Portable Testing Instruments

The surface configuration was determined by means of point gauges supported upon the spacing bars located at each measuring section. These gauges could be read to 1/1000 of a foot, although it was often not possible to take readings with this degree of accuracy, because of the minor disturbances on the high velocity flow surface.

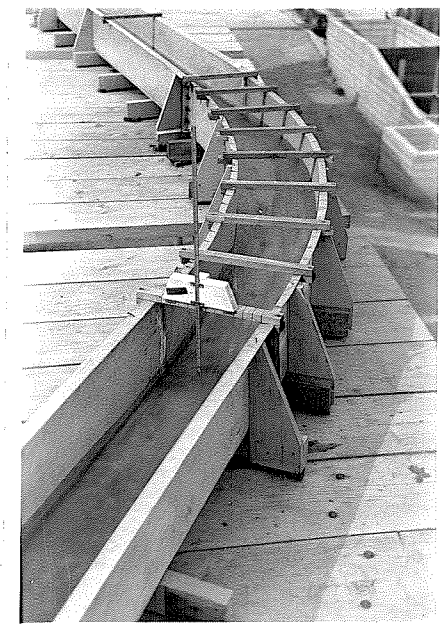

Figure 39 Point Gauge

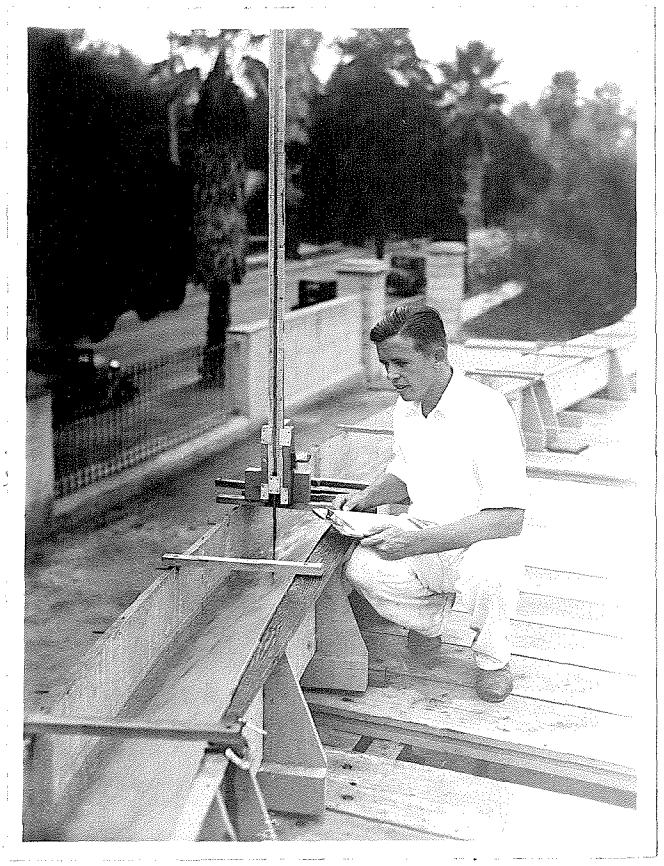

Figure 40 Pitot Measurement

Velocity distributions were obtained by the use of carefully constructed Pitot tubes. These were used at the same stations as the point gauges, the depth and lateral position being determined in the same manner. Velocity readings could be secured as close as 2/100 of a foot from the flume walls.

APPENDIX II

Field Observations on High Velocity Flow in Curves of Rectangular Cross-Section.

Fortunately it was possible during this investigation to secure quite a number of field data on various cases of flow in curved sections of actual flood channels. All these observations leave no doubt as to the fundamental correctness of the principles and conceptions presented in the main part of the thesis. The plotted profiles, of which the best examples are presented on the accompanying drawing, show exactly the same characteristics as they are seen in Figures 9 - 11 of this report, representing cases of the experimental channel. The quantitative evaluation of the field observations meets with some difficulties, since average depth and average velocity cannot be determined so easily and flow conditions do not stay constant during the process of taking data.

(a) Verdugo Wash High Water Marks

Observations of high water marks of Jan. 1, 1934 in a curve of Verdugo Wash below upper Canada bridge were taken by District engineers in August 1935 and presented on drawing no. 10 - ML - 18. Data for this case are:

$b = 43$ feet $\qquad R = 600$ feet

$S = .028$ $\qquad \Theta_o = 12^\circ$ (central angle

$n = .014$ $\qquad$ of curve)

The average depth was interpolated as approximately $d_o = 3.7$ ft.

Then $v_o = 38.1$ ft. per sec.

The maximum depth h' at the outer wall was determined as $h' = 5.8$ ft. at $\theta_o = 12^\circ$. The method of cabulation presented in the report

yields the following results: (as determined by equation 12)

$h' = 6.17$ feet $\qquad\qquad \theta_o = 10^{\circ}6'$

(Note that both the calculated and observed values of h' refer to the mean base line of the channel bottom.)

This agreement is closer than would have been predicted from the degree of accuracy of the field data.

(b) Lower Sycamore Storm Drain

Some observations on water surface profiles were made along the walls of the lower Sycamore storm drain below La Boice Street during the storm of February 12, 1935, by members of the Hydraulic Research Staff of the Los Angeles County Flood Control District. Height gauges had been painted all along the walls about 15 feet apart, which were successively read. These stations extend through two curves of 92 foot radius and $67^{\circ}13'$ central angle and of 212 foot radius and $22^{\circ}27'$ central angle. A number of profiles were read, but the depths of flow reached during that storm were so low that they do not warrant a close analysis. The profiles when plotted show the wave pattern familiar from the other cases. The maximum average depth for a short period of high flow was 2.27 feet, for which, however, only data for the first curve of 92 foot radius could be obtained.

Time of observation, 3:05 - 3:10 P.M.

$d_o = 2.27$ feet $\qquad\qquad Q_{av} = 360$ cu. ft./sec.

$R = 92$ feet $\qquad\qquad v_o = 18$ ft./ sec. (estimated

$b = 9$ feet $\qquad\qquad$ from max. Pitot reading of 21.2 ft./sec.)

Measured maxima:

h'_1 = 2.95 feet $\qquad\qquad$ h'_3 = 3.100 feet

h'_2 = 3.00 feet

Calculated maximum for the above conditions:

h' = 2.94 feet

The complete agreement is of course accidental. The theoretical value of $\theta_o = 8^o40'$ corresponding to a distance from the entrance of 14.1 feet cannot be checked from the measured data, since some inconsistance exists between the data on the beginning of the curve and the beginning of the change in the depths of the entrance sections.

(c) Rubio Storm Drain

The best and most complete field data obtained so far were taken also during the storm of February 12, 1936 by members of the staff connected with the experimental work at the Institute. The observations were taken along the walls of the Rubio Canyon channel below Longden drive. The profiles for maximum discharge are presented in the accompanying drawing. This work was made possible by the Los Angeles County Flood Control District by having depth gauges painted every 20 feet along both channel walls; extending through two curves, the straight section between the curves and that below the second curve. Some float gauge measurements indicate the approximate velocity to have been between 20 - 24 feet per second. Unfortunately discharges obtained from the gauging station in San Gabriel at Broadway cannot be used to full advantage due to the lack of conformity of the time recorded by observers and that of

the automatic gauge. The calculations according to the analytical part of the thesis yield the following results obtained from the average conditions indicated by the plotted profiles. The discharges are taken from the hydrograph, and have been corrected as far as possible for time differences.

1. curve	2. curve
d_o = 2.10 feet	d_o = 2.00 feet
Q = 1200 c.f.s.	Q = 1200 c.f.s.
v_o = 22 ft./sec.	v_o = 23.1 ft./sec.
b = 26 feet	b = 26 feet
R = 445 feet	R = 425 feet
h_1' = 2.9 feet (measured)	h' = 2.9 feet
h_2' = 3.2 feet	
θ_o = 5°10'	θ_o = 8°6'
θ_o = 8°34' (interpolated from position of second max. at θ_2 = 25°42')	
h' = 2.78 feet (calculated using equ. 12.)	h' = 2.8 feet
θ_o = 7°8'	θ_o = 7° 52'

Note: d_o and h' have both been corrected by subtracting .50 feet from the gauge readings. The latter give elevations above lowest point of invert of channel section. Therefore, elevations above mean base line are .50 feet lower. It must be noted also that the entrance conditions to curve (1) are not satisfactory because of the disturbance produced by inflow through a side inlet. This was situated about one hundred feet above the beginning of the curve.

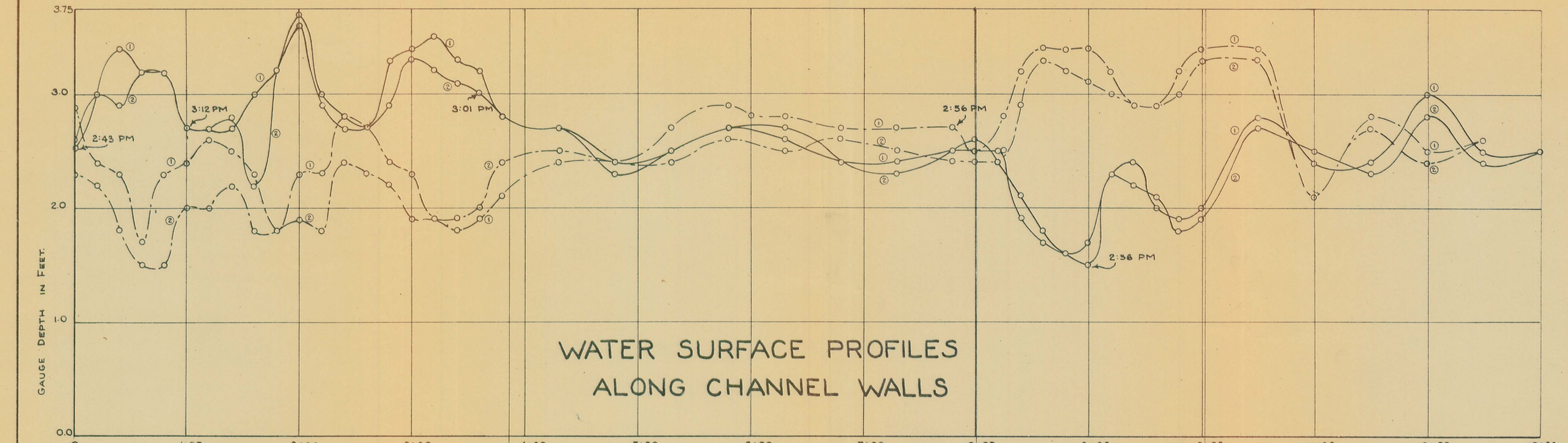

WATER SURFACE PROFILES ALONG CHANNEL WALLS

CHANNEL SECTION

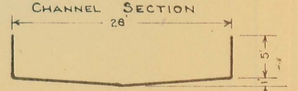

RUBIO WASH BELOW LONGDEN DRIVE

SLOPE = .016 WIDTH = 26.0'

——— RIGHT WALL — · — · — LEFT WALL

LOOKING DOWNSTREAM

TIME	FLOW
2:43 PM	660 CFS
2:56	1,090
3:01	1,350
3:12	1,510

NOTE ~

RUN ① TAKEN GOING DOWNSTREAM

RUN ② TAKEN GOING UPSTREAM

(d) Summary of Field Checks

It should be noted that the above field measurements cover a wide range of conditions, i.e., breadth of channel ranging from 9 to 43 feet, radii of curvature from 92 to 600 feet, and velocities from 18 to 38 feet per second. The results all show remarkably good agreement with the analytical method, especially when it is remembered that the field data are neither complete nor precise. This is especially true as far as measurements of discharge and velocity are concerned. The individual depth measurements are sufficienty accurate but the combined profile suffers from the fact that the discharge did not remain constant over the period of time required to complete the measurements. However, as has been said, the experimental and analytical results are in close agreement despite these difficulties. Therefore it is felt that these results represent a very strong field confirmation of the analytical treatment.

APPENDIX III

Survey of Literature

(a) Literature on High Velocity Flow

1. John R. Freeman: Hydraulic Laboratory Practice
   Publication, A. S. M. E.
   pp. 430 - 431: experiments on air entrainment of Ehrenberger, Vienna, with inclinations of the experimental flume up to 37°.

2. Ph. Forchheimer: Hydraulik
   page 171: 63, Wasserbewegung in steilen Rinnen according to experiments of Ehrenberger. 2 formulae for air entrainment given.

3. R. Ehrenberger: Mitteilungen der Versuchsanstalt fuer Wasserbau Wien, Zeitschrift des Oesterreichischen Ingenieur und Architektenvereins, 78 (1926)
   pp. 155 and 175
   Contains original paper of Ehrenberger on his experiments on air entrainment.

4. Fr. Eisner: Offene Gerinne, Handbuch der Experimental-Physik vol. IV, part 4
   pp. 299 - 301
   Eisner quotes Bazin's experiments on supercritical flow.

5. E. W. Lane: Recent studies on flow conditions in steep chutes, Engg. News Rec. 1936, Nov. 1
   pp 5 - 7, 6 fig.
   Lane presents qualitative considerations, no formulae, roughness investigated.

(b) Literature on subcritical flow in curves

1. Ph. Forchheimer: Hydraulik, 1930
   page 310
   Forchheimer quotes mainly ideas and analysis of Y. Boussinesq, which were originally presented in Eaux courantes, p. 602 and in Journ. de Mathem. 9, 1883, p. 129.
   Boussinesq considers a curve as a series of sharp bends and gives form of expression for loss of head in curves.

2. S. M. Woodward: Hydraulics of the Miami Flood Control Project, Technical reports, part VII, 1920. page 271
   Customary formula for superelevation and some better mathematical approaches.

Survey of Literature (cont.)

b. 3. H. C. Ripley: Relation of depth to curvature of channels, Trans. A. S. C. E. 1927, pp. 207 - 267 with discussion. Ripley treats curvature effect on depth and profile of rivers with erodable beds. He quotes a formula of the French engineer Gockinga for calculation of superelevation.

This survey shows the scarcity of information available on high velocity flow in steep channels and the complete lack of a treatment of high velocity flow with regard to curved channels.